Journal of
Medicinal Chemistry

Article

BENZOTHIAZOLE-BASED LRRK2 INHIBITORS AS WNT ENHANCERS AND PROMOTERS OF OLIGODENDROCYTIC FATE

Josefa Zaldivar-Diez, Lingling Li, Ana M. Garcia, Wenning Zhao, Cristina Medina-Menendez, Stephen J. Haggarty, Carmen Gil, Aixa V. Morales, and Ana Martínez

J. Med. Chem., **Just Accepted Manuscript** • DOI: 10.1021/acs.jmedchem.9b01752 • Publication Date (Web): 11 Dec 2019

Just Accepted

is published by the American Chemical Society. 1155 Sixteenth Street N.W., Washington, DC 20036

REVISED 5 12.11.2019

BENZOTHIAZOLE-BASED LRRK2 INHIBITORS AS WNT ENHANCERS AND PROMOTERS OF OLIGODENDROCYTIC FATE

Josefa Zaldivar-Diez,[1] Lingling Li,[2] Ana M. Garcia,[1] Wen-Ning Zhao,[3] Cristina Medina-Menendez,[2] Stephen. J. Haggarty,[3] Carmen Gil,[1,4] Aixa V. Morales,[2*] Ana Martinez[1,4*]

[1] Centro de Investigaciones Biológicas-CSIC, Ramiro de Maeztu 9, 28040 Madrid (Spain)

[2] Instituto Cajal-CSIC, Av. Doctor Arce, 37, 28002 Madrid (Spain)

[3] Chemical Neurobiology Lab, Center for Genomic Medicine, Departments of Neurology and Psychiatry, Massachusetts General Hospital, Harvard Medical School, 185 Cambridge Street, Boston, MA 02114 (USA)

[4]Centro de Investigación Biomédica en Red de Enfermedades Neurodegenerativas (CIBERNED), Instituto Carlos III, 28031 Madrid (Spain).

*Correspondence to:

Prof A Martinez (ana.martinez@csic.es)

Dr A. V. Morales (aixamorales@cajal.csic.es)

Abstract

Leucine Rich Repeat Kinase 2 (LRRK2) is an enigmatic enzyme and a relevant target for Parkinson's Disease (PD). However, despite the significant amount of research done in the last decade, the precise function of LRRK2 remains largely unknown. Moreover, the therapeutic potential of its inhibitors is in its infancy with the first clinical trial having just started. In the present work, the molecular mechanism of LRRK2 in the control of neurogenesis or gliogenesis was investigated. We designed and synthesized novel benzothiazole-based LRRK2 inhibitors and showed that they can modulate the Wnt/β-catenin signaling pathway. Furthermore, compounds **5** and **14** were able to promote neural progenitors proliferation and drive their differentiation towards neuronal and oligodendrocytic cell fates. These results suggest potential new avenues for the application of LRRK2 inhibitors in demyelinating diseases in which oligodendrocyte cell-death is one of the pathological features.

Keywords: LRRK2 inhibitors, adult neurogenesis, Wnt enhancers, oligodendrocyte differentiation

Introduction

Leucine Rich Repeat Kinase 2 (LRRK2) is an enigmatic enzyme that is considered one of the most attractive targets for Parkinson's Disease (PD).[1] Since its discovery in 2004,[2] LRRK2 research has progressed significantly in recent years with a growing number of reports of LRRK2 interactors and more selective and potent LRRK2 kinase inhibitors.[3] However, the potential pathophysiological roles of LRRK2 is much more complicated and it can be related to other neurodegenerative disorders, opening the translational potential of its inhibitors beyond PD. It is crucial to take into consideration that LRRK2 functions have been mainly studied in neurons, where the expression of endogenous LRRK2 is low, and therefore, more studies are needed to have a better understanding of the role played by LRRK2 inside and outside the central nervous sytem (CNS).

LRRK2 is considered to be a large protein constituted of 2527 amino acids and classified as a member of the ROCO superfamily, which is characterized by the presence of a Ras/GTPase C-domain (ROC), a kinase domain and a carboxy-terminal of Roc sequence (COR), which linking them together.[4] In addition, domains related to protein-protein interaction are found: the N-terminal region of LRRK2 is formed by the armadillo (ARM) domain,[5] the ankyrin (ANK) domain comprising seven ankyrin-type repeats, thirteen leucine-rich repeats in the LRR domain,[6] followed by the catalytic domain with both GTPase and activity (ROC-COR-Kinase) and finally the WD40 domain, which consists of C-terminal repeats.[7]

The physiological functions of LRRK2 have been largely related to its two enzymatic activities: the kinase domain that catalyzes phosphorylation and the ROC-GTPase domain that is involved in GTP-GDP hydrolysis. In addition to those catalytic

functions, multiple protein-protein interaction regions indicate that LRRK2 may act as a scaffolding protein contributing to the formation of a multiprotein signaling complex.[8] A step forward in understanding the physiological role of LRRK2 was the discovery of Rab GTPases as substrates of LRRK2 catalytic activity.[9] Additionally, growing evidence implicates LRRK2 function in remarkably diverse pathways, which involve the regulation of transcription,[10] regulation of translation,[11] mitochondrial function,[12] neurite outgrowth,[13] cytoskeletal dynamic,[14] vesicle trafficking,[15] autophagic protein degradation,[16] inflammation[17] and regulation of adult neurogenesis.[18]

In a previous work from our group,[19] we presented a new family of indolinone-like LRRK2 inhibitors that showed a proneurogenic effect as they increased the proliferation rate of neural precursor cells isolated from adult mice ventricular-subventricular zone. However, it is unknown what the underlying molecular mechanism of LRRK2 in the control of neurogenesis or gliogenesis entails and if LRRK2 regulates the generation of new neurons or glial cells in the context of adult brain. One of the possible mechanisms could be through the control of Wnt/β-catenin signaling pathway. Wnt/β-catenin signaling is known as one of the major players in all stages of brain development[20] and in the generation of new neurons and oligodendrocytes in the adult brain.[21-22] Using a Wnt signaling reporter mouse,[23] Wnt/β-catenin signaling activity has been observed in neural stem cells and neural progenitor cells of the ventricular-subventricular zone (V-SVZ). Also, Wnt/β-catenin activity is upregulated as an endogenous repairing mechanism in ischemic stroke[24] and traumatic nerve injury models.[25]

Growing evidence suggests that deficiencies in Wnt signaling in the adult brain may be linked to the etiology of several neurodegenerative diseases.[26] Furthermore, Wnt/β-catenin activation with specific small molecules modulators, such as some glycogen synthase kinase-3β (GSK-3β) inhibitors, has been shown to promote neuroregeneration

in ageing mouse models of PD by rescuing midbrain dopaminergic stem cells.[27] Taken together, these data suggest that pharmacological modulation of the Wnt signaling in the adult brain might lead to new therapeutic strategies for neurological diseases.[28]

LRRK2 plays a key role in Wnt signaling,[29] with reported direct physical interactions between low-density lipoprotein receptor-related protein 6 (LRP6), the cytoplasmic phosphoproteins known as DVL1 (Dishevelled 1) and components of the β-catenin destruction complex.[30] Pathogenic mutations in LRRK2 (R1441C, Y1699C and G2019S) weakened those interactions with Wnt pathway components,[31] while recently, the gain-of-function LRRK2 mutations have been demonstrated to enhance the repression of β-catenin signaling[32] showing the involvement of this kinase in canonical Wnt pathway.[33]

Based on this collective evidence, we aimed to find new chemically diverse LRRK2 inhibitors that could be used in a chemical genetic approach for a deep interrogation of the role of LRRK2 in adult neurogenesis. The goal was to have pharmacological tools able to probe the induction of Wnt signaling in human cells and to determine their potential as regulators of adult neurogenesis using neural stem cells isolated from the neurogenic niche of adult mouse V-SVZ both in proliferation and in differentiation experiments. In this work, we present a class of promising novel LRRK2 inhibitors that fulfill these characteristics and therefore may open new indications for LRRK2 inhibitors outside the PD spectrum.

Results and discussion

Design and synthesis of new compounds

Previous reported computational studies of LRRK2,[34] led to the identification of two hits (**1-2**) together with their main interactions with the protein due to a pair of strong

hydrogen bonds and a number of hydrophobic interaction. With these results in mind, we designed a small series of amino[6+5]benzo-annelated compounds with a phenyl-morpholino tail able to maintain these main interactions (Figure 1). Following a convergent synthesis pathway, derivatives **3-5** were easily obtained as described in the experimental section, and evaluated as LRRK2 inhibitors using a commercial methodology.[35] The three new compounds differ in the heteroatoms in the heterocyclic framework. Remarkably, when the heteroatom was a sulfur atom, promising activity was found. In fact, benzothiazole **5** showed an IC_{50} value of 0.70 μM for LRRK2 inhibition and was considered as a new lead for further optimization (Figure 1).

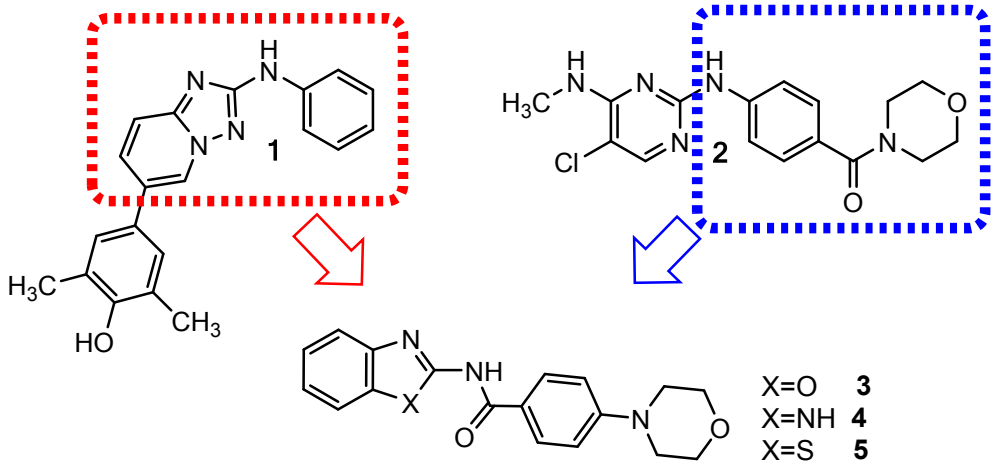

Figure 1. Design of the first LRRK2 inhibitors.

Several structural modifications of benzothiazole **5** were proposed including substituents with different steric and electrostatic chemical properties in different positions of the heterocyclic ring together with the replacement of the morpholino moiety by tails of different nature (Figure 2).

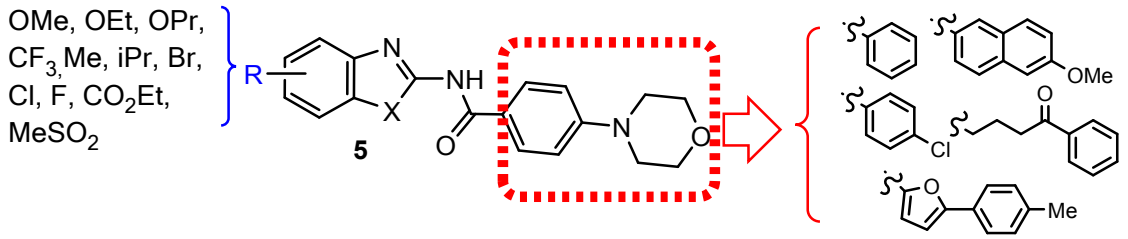

Figure 2. Proposed modifications for benzothiazole **5**.

The synthesis of the *N*-(benzothiazol-2-yl)-4-morpholinobenzamide derivatives was performed by a coupling reaction between the corresponding 2-amino-benzothiazole and the 4-morpholinobenzoic acid (Scheme 1). Each 2-amino-benzothiazole was mixed with the 4-morpholinobenzoic acid in the presence of 1-ethyl-3-(3-dimethylaminopropyl)carbodiimide (EDCI) as a coupling agent and 4-dimethyl-aminopyridine (DMAP) as a basic catalyzer. Previously, the 4-morpholinobenzoic acid was activated with the coupling agent for a certain time and then the corresponding 2-amino-benzothiazole was added. Following this procedure, it was possible to obtain the corresponding *N*-(benzothiazol-2-yl)-4-morpholinobenzamide derivatives with low to moderate yields (<50%). A total of thirteen new benzothiazoles (**6**-**17**) were synthesized with different substituents in the benzo-annelated ring in order to see the influence of their nature and position in the biological activity. In an attempt of increasing the reaction yield, a different methodology was assayed for the synthesis of compound **18**. For that purpose, we used (benzotriazol-1-yloxy)tripyrrolidinophosphonium hexafluorophosphate (PyBOP) and 1-hydroxybenzotriazole (HOBt) with the 4-morpholinobenzoic acid, dissolved in THF to activate the acid under microwave irradiation (50 ºC) during 1 hour and then adding the corresponding amino-benzothiazole and heating the resulting mixture during 5 hours at 110ºC under microwave irradiation. However, the yield was similar to the previous conditions used.

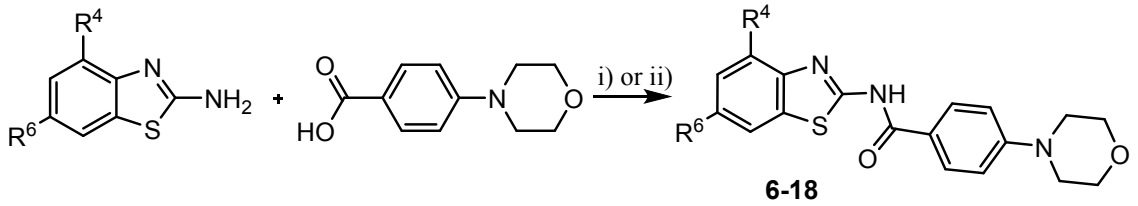

Scheme 1. i) EDCI, DMAP, Et_3N, CH_2Cl_2, r.t., ii) PyBOP, HOBt, MW (110 °C, 5h), THF

To study the influence of the morpholino moiety in the kinase inhibition and to confirm the relevance of this chemical fragment in the biological activity, the synthesis of *N*-(6-flurobenzothiazol-2-yl)-benzamide derivatives (**19-23**) was proposed and executed following the methodologies described above (Scheme 2).

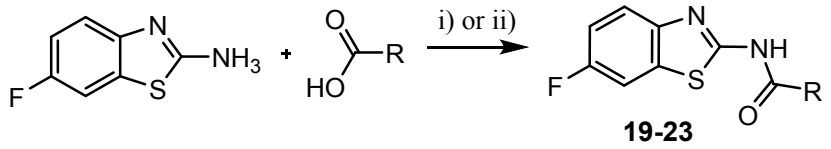

Scheme 2. i) EDCI, DMAP, Et_3N, CH_2Cl_2, r.t., ii) PyBOP, HOBt, MW (110 °C, 5h), THF

The chemical structures of all the newly synthetized compounds were assigned unequivocally based in their analytical and spectroscopic data (see experimental section).

LRRK2 inhibition, SAR and docking studies

The potential LRRK2 inhibition was evaluated for all the new benzothiazole derivatives **5-23**. When some activity was found, the compounds were also tested as potential inhibitors of LRRK2 G2019S, a superactive kinase form carrying the most common LRRK2 mutation found in familial PD patients.[36] The assays were performed using a fluorescent-based immunoassay for the detection of ADP formed by the kinase reaction.[35] Initially all the compounds were evaluated at a fixed concentration of 10 μM, and the dose response curves were obtained and IC_{50} values calculated only for those

compounds showing higher than 50% inhibition. Only when the compounds showed inhibition on the wild type LRRK2, the potential inhibitory activities on the mutant LRRK2 G2019S were assayed. Results are depicted in Table 1 using the known LRRK2 inhibitor Lrrk2-in-1 as reference standard.[37]

Table 1. LRRK2 enzymatic activity, permeability (P*e*) in PAMPA-BBB assay and Wnt signal enhancement expressed as normalized fold change to DMSO of benzothiazole compounds **5**-**23**.

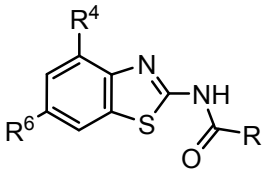

Comp	R^4	R^6	R	LRRK2 %inh@ 10µM	LRRK2 IC_{50} (µM)[a,b]	LRRK2 G2019S %inh@ 10µM	LRRK2 G2019S IC_{50}(µM)[a,b]	P*e* 10^{-6}cm.s^{-1}	Fold increase Wnt 1µM	Fold increase Wnt 10µM
5	H	H	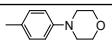	75%	0.70 ±0.13	85%	0.37±0.01	13.4±2.4 CNS+	3.25	2.20
6	H	OMe	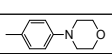	73%	0.37±0.01	93%	0.44±0.29	n.d.	-	-
7	H	CF_3	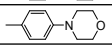	51%	2.27±1.32	69%	0.28±0.10	n.d.	-	-
8	H	Me	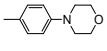	61%	0.48±0.03	71%	0.33±0.07	19.0±2.6 CNS+	1.76	1.79
9	H	Cl	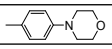	60%	0.37±0.06	50%	-	-	-	-
10	H	F	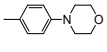	66%	0.17±0.03	55%	0.18 ±0.05	5.1±0.1 CNS+	1.58	2.00
11	Me	H	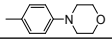	18%	-	-	-	-	-	-
12	Cl	H	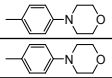	32%	-	-	-	-	-	-
13	H	OEt	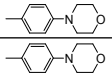	80%	0.30±0.06	85%	0.16±0.02	n.d.	-	-
14	H	Br	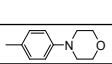	75%	0.51±0.14	70%	0.26±0.15	4.2±0.1 CNS+	1.25	2.00
15	H	OPr	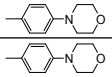	13%	-	-	-	-	-	-
16	H	^{i}Pr	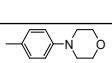	48%	3.49±0.52	70%	1.12±0.43	4.3±3.4 CNS+	1.19	1.22
17	H	SO_2Me		77%	2.50±0.76	80%	0.98±0.17	4.3±2.7 CNS+	1.85	1.86
18	H	CO_2Et	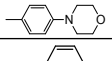	22%	-	-	-	-	-	-
19	H	F		81%	0.52±0.08	79%	0.52±0.08	15.0±1.3 CNS+	1.43	2.29
20	H	F		68%	4.46±0.97	67%	5.64±1.88	n.d.	-	-
21	H	F		13%	-	-	-	-	-	-
22	H	F		16%	-	-	-	-	-	-
23	H	F	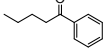	11%	-	-	-	-	-	-

[a] standard compound Lrrk2-in-1: IC_{50} values: 0.02 µM and 0.02 µM in LRRK2 and LRRK2 G2019S respectively, [b] IC_{50}Values ± Standard deviation (ten different concentrations per compound, in two independent experiments) Origin 9.0 software used; n.d.: not possible to determine in the experimental conditions

The great majority of the newly prepared compounds were able to inhibit LRRK2 in the submicromolar range being equipotent or at times having enhanced inhibition with the mutant superactive LRRK2 G2019S form. Structure-activity relationships studies pointed to a complete lack of activity when a substituent was attached to the position 4 of the benzothiazole moiety (see compounds **11** and **12** *versus* **8** and **9**) or when a phenyl ring was not attached to the carbonyl linker (see compounds **21**-**23** versus **19**-**20**).

In order to gain insight into the binding mode of these benzothiazole-based LRRK2 inhibitors, a docking study using Glide XP (Schrödinger suite program) that allows examination of a potential binding mode to the enzyme was carried out. Although the kinase domain of LRRK2 has not been crystallized, a LRRK2 homology model has been published[34] and we have reproduced it and used with success in previous work.[19] All the compounds showed a similar binding mode and the structure-activity relationships could be easily explained. Derivative **10** is the one that shows the highest activity in the wild type form of LRRK2 (IC_{50}=0.19 μM). The nitrogen in the benzothiazole core is able to form a hydrogen bond with Asp2017 in the catalytic site. Furthermore, the fluorine atom at position 6 of the benzothiazole may form a halogen bond with Glu1920. In addition, the side chain of Arg1957 is flexible and it may, therefore, form a hydrogen bond with the oxygen atom of the morpholino moiety (Figure 3A).

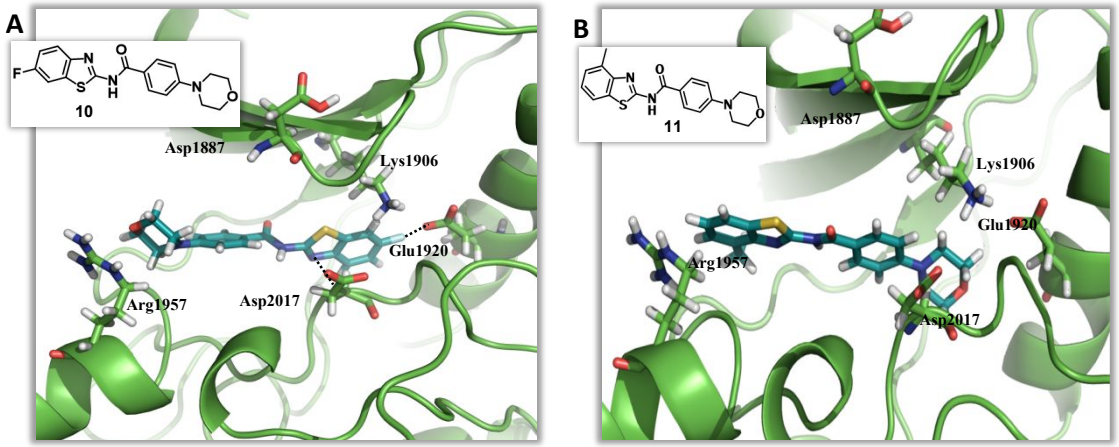

Figure 3. (A) Docking of compound **10** in the LRRK2-homology model. Dashed lines show hydrogen-bonds and halogen-bonds. **(B)** Docking of benzothiazole **11**.

However, when substitution takes place at position 4 of the benzothiazole moiety instead of position 6, activity dramatically decreases (see **11-12** *vs* **8-9**). This lack of activity could be explained based on steric hindrance: the benzothiazole core is not able to fit inside the cavity, therefore, the phenyl-morpholino moiety is the part of the molecule allocated towards the cavity whereas the benzothiazole core is oriented to the external part exposed to the solvent. In this last binding mode, interactions with Glu1920, Arg1957 and Asp2017 are lost (Figure 3B). The docking of compound **11** is shown as an example.

Regarding the nature of the substituent in the exocyclic nitrogen atom, both morpholino or phenyl moieties were allowed by the enzyme (see **10**, **19**, **20** *vs* **21-23**). The docking of **19** is shown as an example (Figure 4A). However, when the moiety attached to exocyclic nitrogen is bigger and/or it contains more than one aromatic ring it results in a lack of activity. Docking of compound **21** is shown as an example, and in this case, the loss of activity could be explain that in order to allocate the aliphatic chain attached to the exocyclic nitrogen the benzothiazole core changes its orientation: the nitrogen atom is now pointed to the exterior of the cavity and the sulphur atom towards the interior. With this binding mode, both the hydrogen-bond between the nitrogen and Asp2017

and the halogen-bond between the fluorine and Glu1920 are impossible to be formed (Figure 4B).

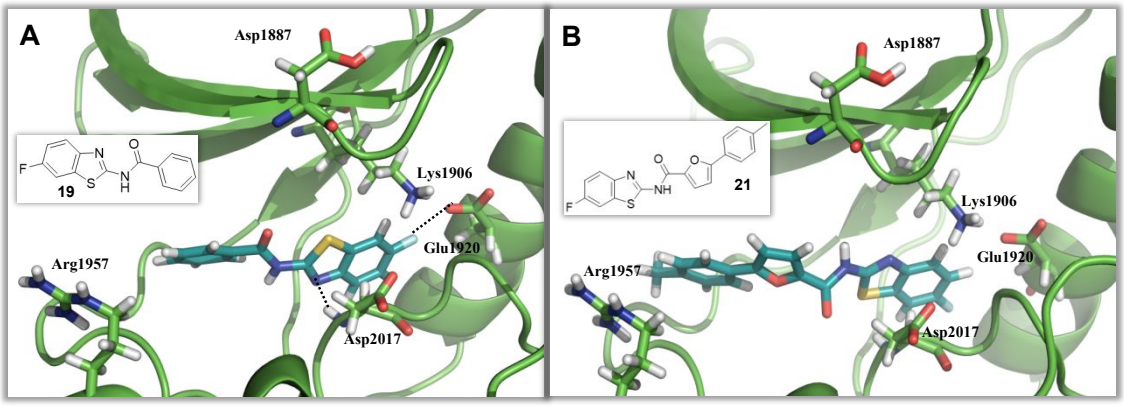

Figure 4. (A) Docking of compound **19** in the LRRK2 homology model. Dashed lines show hydrogen-bonds and halogen-bonds. **(B)** Docking of compound **21** in the homology model.

These docking studies performed can be used to further optimize this family of compounds in a lead-to-candidate process. The introduction of halogens in position 5 of the benzothiazole core can be studied to determine if two halogen-bonds with the enzyme could be formed and thus increase the enzymatic activity.

Prediction of blood-brain barrier (BBB) penetration

Blood-brain barrier (BBB) penetration is an essential drug-like property for any compound developed to target neurodegenerative and neurological diseases. Here, we used a Parallel Artificial Membrane Permeability Assay (PAMPA) as a high throughput technique to predict the passive permeability into the brain of the biological active benzothiazole derivatives that were synthesized.[38] We employed a brain lipid porcine membrane in the assay. The *in vitro* permeability (*P*e) of ten commercial drugs through lipid membrane extract together with the tested compounds was determined. An assay validation was made comparing the reported permeability values (*P*e*)* of human commercial drugs with the experimental data obtained (Table S1). A good correlation between experimental-described values was obtained *P*e (exp) = 1.3711 (bibl) – 1.4509

(R^2= 0.972) (Figure S1). From this equation and following the pattern established in the literature for BBB permeation prediction,[39] compounds could be classified as CNS+ when they present a permeability > 4.03 x 10^{-6} cm.s^{-1}. Based on these results compounds **5**, **8**, **14, 10**, **16**, **17** and **19**, with *P*e values in that range, are predicted to be able to cross the BBB by passive permeation (Table 1). In contrast, compounds **6**, **7**, **13** and **20** precipitated in the experimental conditions employed or lacked a clear UV spectrum after filtration. Thus, it was not possible to determine their BBB permeability prediction using this methodology.

Wnt signaling modulation

The pharmacological modulation of Wnt signaling is very relevant for inducing the generation of new neurons and glial cells in the aging or neurodegenerative adult brain.[40] LRRK2 has been shown to repress canonical Wnt signaling acting in interaction with key Wnt signaling components (DVL1, LRP6, amongst others), whereas many of the pathogenic mutated forms of LRRK2 (R1441C, G2019S) decrease, even more, Wnt signaling activity.[31] Therefore, we tested the LRRK2 inhibitors synthesized here and found to be predicted as BBB penetrant (Table 1) in a high-throughput-screen to determine their ability to promote Wnt modulation. For that purpose, we used human neural progenitor cells (NPC), derived from induced pluripotent stem cell (iPSC), that stably express a TCF/LEF-luciferase reporter gene to monitor Wnt signaling activity.[41] The expression of LRRK2 was confirmed by quantitative RT-PCR both in the iPSCs and in the NPC line used (Figure 5).

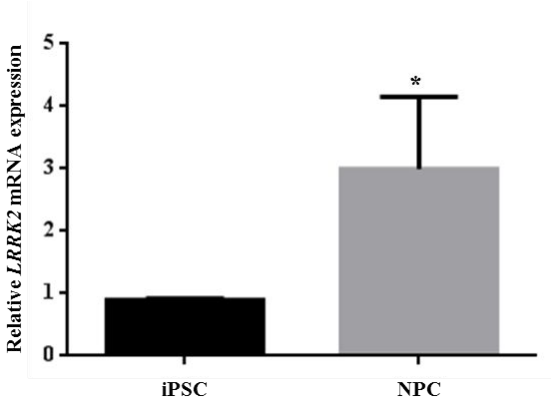

Figure 5. Real time RT-PCR of LRRK2 expression in induced Pluripotent Stem Cells (iPSC) and Neural Progenitor Cells (NPC). Quantitative values were normalized to iPSC (set to 1) and GAPDH. Values represent averages of triplicates. Error bars indicate standard deviations (SD) of the mean. *p≤ 0.05

Compound activity was assessed in the presence of Wnt3a protein delivered as Wnt3a-expressing cells conditioned media. Compounds were tested at two fixed concentrations of 1 and 10 μM and the results were expressed in fold increase of TCF/LEF reporter activity with respect to vehicle DMSO as control (Table 1).

In all the assayed compounds a modest, but consistent increase of Wnt signaling was observed. Compounds **5**, **10**, **14** and **19** showed more than two fold change in Wnt activity and were selected to perform dosage dependent curves from 0.01 μM to 20.00 μM. The assay was performed in the same way as before but this time serial dilutions of the compounds were used and each concentration of individual compound was repeated eight times. Results were expressed in average fold increase of TCF/LEF reporter activity with respect to that of DMSO ± SD and plotted in dose-dependent curves. CHIR-99021, a GSK3β inhibitor and consequently a strong positive modulator of Wnt signaling, was used as reference control (Figure 6).[42]

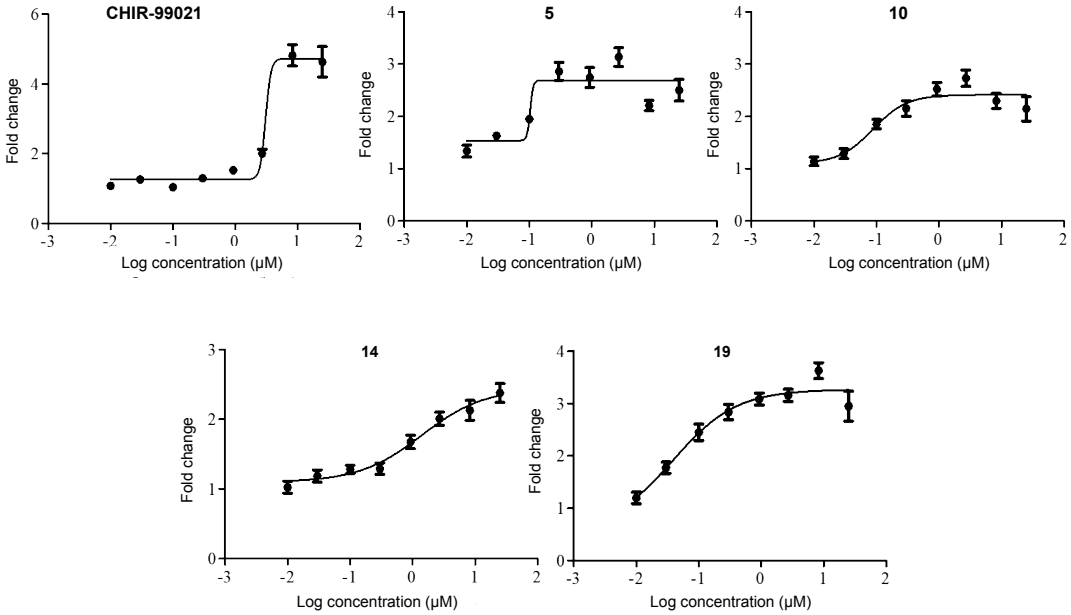

Figure 6. Dose-dependent curves of Wnt modulation (y axis represents fold change and x axis compound concentration) of compounds **5**, **10**, **14** and **19** and CHIR-99021 as positive control.

We noted that a number of the observed dose responses showed steep hill coefficients, i.e. compounds went from showing little activity to a rapid increase in activity upon increasing the dose. This was particularly the case of the reference control GSK3 inhibitor CHIR99021 and compound **5**, while compounds **10, 14** and **19** show a more traditional concentration-dependent effect on Wnt pathway activity. Together, we observed a clear correlation between the concentration of the compound and the fold-change in Wnt activity. Together, these experiments demonstrate that benzothiazole-based LRRK2 inhibitors produce a modest, but dose-dependent increase of Wnt/β-catenin signaling in human NPCs. These data suggest that LRRK2's kinase activity may function to repress Wnt signaling. Mechanistically, since we measure changes in transcription through a TCF/LEF-dependent reporter gene we surmise the inhibition of LRRK2 leads to accumulation of nuclear β-catenin leading to transcriptional induction.

Finally and to assess the modulation of Wnt signaling pathway, Axin-2 mRNA expression, one of the known Wnt/β-catenin direct target genes, was quantified for compounds **5**, **10**, **14** and **19**. In all the cases we have observed an increase in mRNA levels which confirms the activation of Wnt signaling activity previously determined (Figure 7). The four inhibitors tested have an IC_{50} value in LRRK2 inhibition in the same range of activity. Thus, differences on Axin-2 expression may be associated to the different physico-chemical properties of each compound that may influence in solubility, cell penetration, protein binding, etc. This moderate Wnt signaling promotion, exhibited by our benzothiazole-based LRRK2 inhibitors, could be very relevant to rescue the pathogenic LRRK2 activity in neurodegenerative diseases where Wnt signaling is impaired.

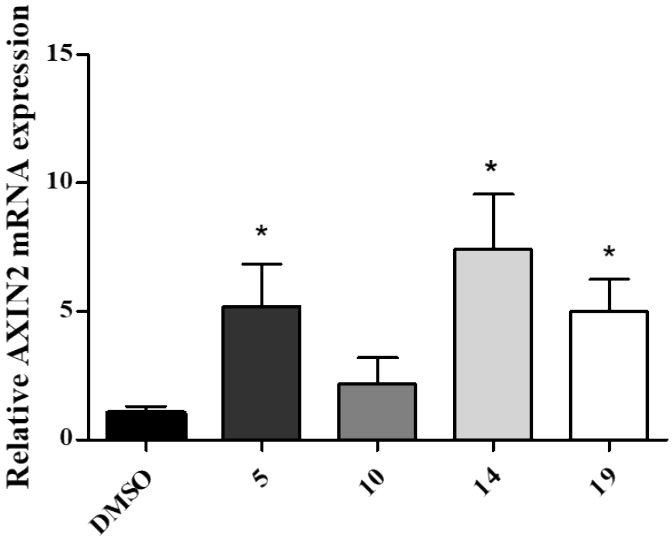

Figure 7. Real time RT-PCR of Axin2 expression in Neural Progenitor Cells (NPC) of compounds **5**, **10**, **14** and **19**. Quantitative values were normalized to DMSO (set to 1) and GAPDH. Values represent averages of triplicates. Error bars indicate standard error of the mean (SEM).. *p≤ 0.05

Additionally, the standard Wnt reporter assay was also run at basal condition (without adding Wnt3a) (data not shown). In this condition, our compounds did not have activity on their own consistent with the fact that like many compounds in human iPSC-derived

NPCs there is often a requirement for co-stimulation with a Wnt ligand to observe strong activation. The fact that the compounds do not activate the reporter on their own also provides a functional signature that distinguishes them from other classes of known Wnt pathway activators tested in the same assay, including GSK-3 and HDAC inhibitors, as both activate basal Wnt signaling and enhance the effects of adding Wnt3a. Thus, the lack of activity of the compounds on their own provides a measure of specificity of the compounds.

Neurogenic properties of LRRK2 inhibitors

Adult NSCs continuously generate neurons throughout life in two main brain regions: the subgranular zone of the hippocampus and the V-SVZ, adjacent to the lateral ventricles.[43] The V-SVZ is the largest germinal region in the adult mammalian brain and generates olfactory bulb interneurons and oligodendrocytes. Moreover, in human brain, it can be the source of the neuroblasts and interneurons found in the adjacent striatum.[44] Thus, the finding of new molecules able to increase the neurogenic potential of the V-SVZ niche, is of great relevance. Although LRRK2 expression has been described in different brain regions such as cortex, *substantia nigra*, caudate putamen, olfactory bulb and hippocampus, amongst others,[45] it has been poorly described in neurogenic niches.[46] To clarify which cells of the V-SVZ niche of the adult brain could express LRRK2, we performed immunohistochemical analysis in 2.5 months old mice brain coronal sections. Within the V-SVZ, glial fibrillary acidic protein (GFAP)-positive type B cells with hallmark features of astrocytes are neural stem cells and have multipotent self-renewing capacity *in vitro*.[43]

LRRK2 is clearly expressed in most of the NSCs or type B cells with radial-like morphology expressing GFAP and Sox2 (Figure 8A and 8B) while only a

subpopulation of neuroblasts or type A cells, doublecortin (Dcx) positive cells expresses LRRK2. Furthermore, we confirmed that LRRK2 was also expressed in the subgranular zone of the dentate gyrus (Figure 9). Altogether, these results suggest a possible involvement of this kinase in the control of the neurogenic process as it is present in both adult brain niches.

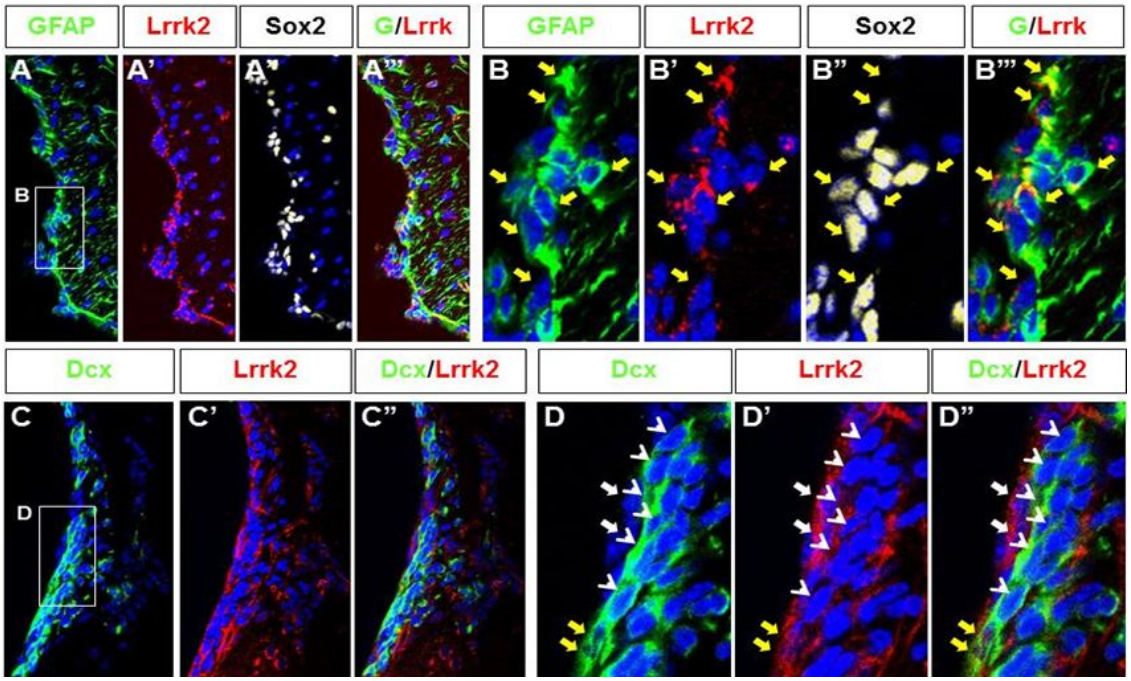

Figure 8. (A, B) Coronal sections of a 2.5 months old brain mouse showing expression of GFAP (green) and Sox2 (white) in radial glia-like NSCs in the SVZ of the lateral ventricles. The majority of those cells coexpress LRRK2 (red, yellow arrows). **(C, D)** Similar sections showing Dcx expression (green cells, arrowheads) in neuroblasts cells. LRRK2 is expressed in the same neurogenic area (red cells, white arrows) but only in few neuroblasts was coexpressed with Dcx (yellow arrows). The nuclei were stained with bisbenzimide (blue) in all the panels. A total of three mice (2 males and 1 female) were used.

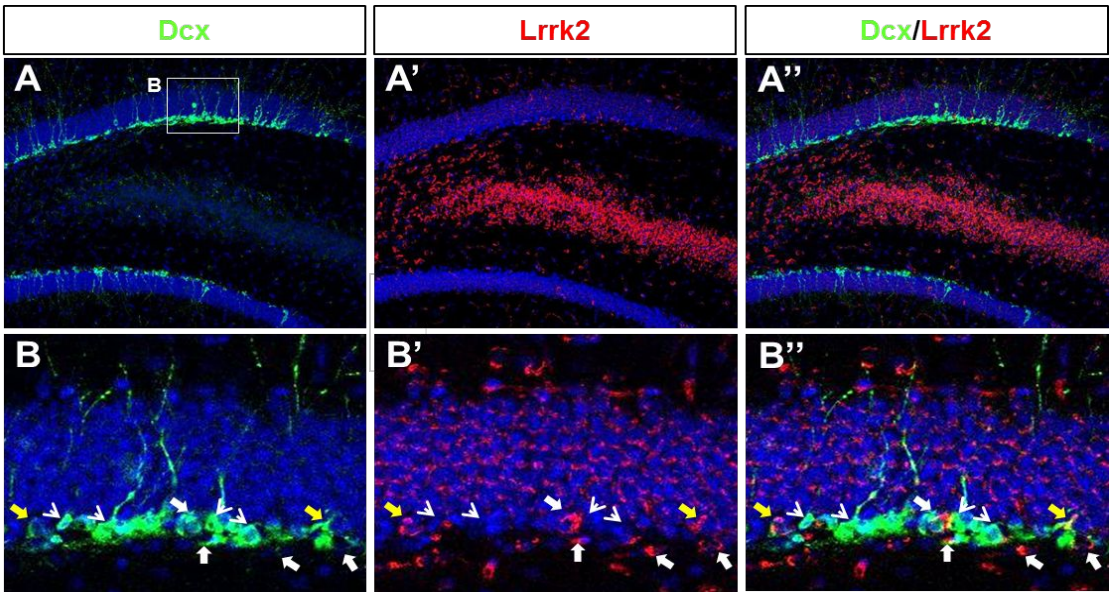

Figure 9. **Expression of LRRK2 in the DG of the hippocampus in the adult mouse brain. (A, B)** Coronal sections of a 2,5 months old brain mouse showing Dcx expression (green cells, arrowheads) in neuroblasts cells and immature granule cells in the subgranular zone of the dentate gyrus (DG). LRRK2 is also expressed in cells of the subgranular zone (red cells, white arrows), including Dcx expressing cells (yellow arrows). LRRK2 is also expressed by cells in the Hilus (Hi) and in pyramidal neurons of the CA3 region of the hippocampus. . A total of three mice (2 males and 1 female) were used.

As modulation of Wnt signaling could have an impact on neurogenesis, we evaluated in a neurosphere proliferation assay the new LRRK2 inhibitors that positively impact on Wnt pathway. We used an *in vitro* neurospheres culture model derived from NSCs and neural progenitors.[47] The V-SVZ of adult mice was employed to isolate the above mentioned stem cells. These primary cells were cultured with and without the selected LRRK2 inhibitors at two concentrations (1 and 5 μM) using the selective and brain permeable LRRK2 inhibitor PF06447475 (PF-475) as control.[48] In the first step, we determined the potential effect of the selected LRRK2 inhibitors on the formation of neurospheres grown for 4 days in the presence of mitogens (FGF and EGF). The size of neurospheres (estimated as total area of the neurospheres) was significantly higher in those cultures treated with the selected small molecules compared to controls treated with DMSO (Figure 10).

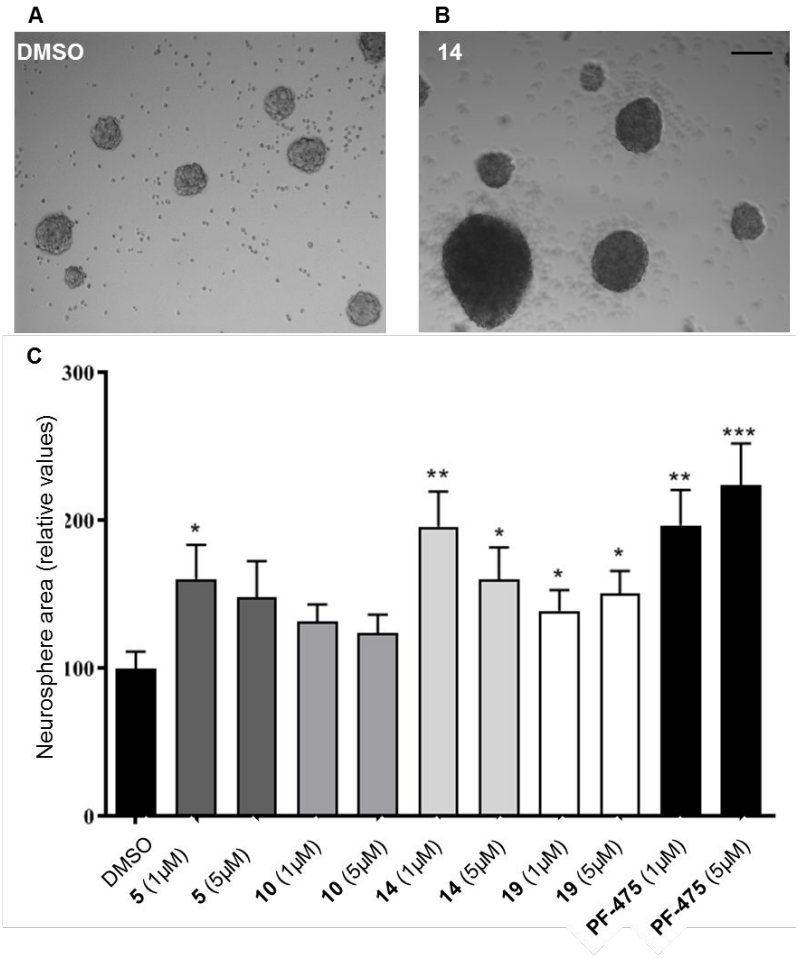

Figure 10. LRKK2 inhibitors promoted proliferation of NSCs and progenitors from adult V-SVZ. Representative bright field micrographs showing the size of primary neurospheres after 4 days in culture in the presence of DMSO as a control **(A)** or LRRK2 inhibitor **14** (**B**). **(C)** Quantitative analysis of the neurospheres in culture. The total neurosphere area was measured in each field using an especially designed macro for IMAGE J. Results are mean values ± standard error of the mean (SEM), represented as relatives to control value (=100), of 6 different fields each one from triplicates and from three independent experiments. *p≤0.05; **p≤0.005. Neurospheres were prepared separately in three experiments from a total number of four mice (2 females and 2 males).

The increase, ranging from 1.8- to 2.4-fold in the total area of the formed neurospheres, was a reflection of the proliferating capacity of the NSCs and neural progenitors that form the neurospheres. Thus, treatment with benzothiazole-based LRRK2 inhibitors promotes the proliferation of NSCs and neural progenitors from adult SVZ.

In order to determine whether the most promising LRRK2 inhibitors (**5** and **14**) could be acting through the modulation of Wnt signaling pathway, we performed neurospheres proliferation experiments in the presence of a widely used Wnt signaling inhibitor, XAV-939. This compound selectively inhibits Wnt/β-catenin-mediated transcription through tankyrase1/2 inhibition, and thus, XAV-939 increases the protein levels of the Axin-GSK3β complex and promotes the degradation of β-catenin.

Adult SVZ-derived neurospheres grown in the presence of 1 μM XAV-939 for 4 days, showed a 30% decrease in their size in comparison with control DMSO treated cells, as expected for a Wnt signaling inhibitor (Figure 11). Moreover, the proliferating activity promoted by LRRK2 inhibitors **5** and **14** was completely reverted in the presence of the Wnt signaling inhibitor XAV939 (Figure 11). In conclusion, our benzothiazole-based LRRK2 inhibitors may promote the proliferation of adult NSCs and neural progenitors, at least in part, through the activation of Wnt/β-catenin signaling pathway.

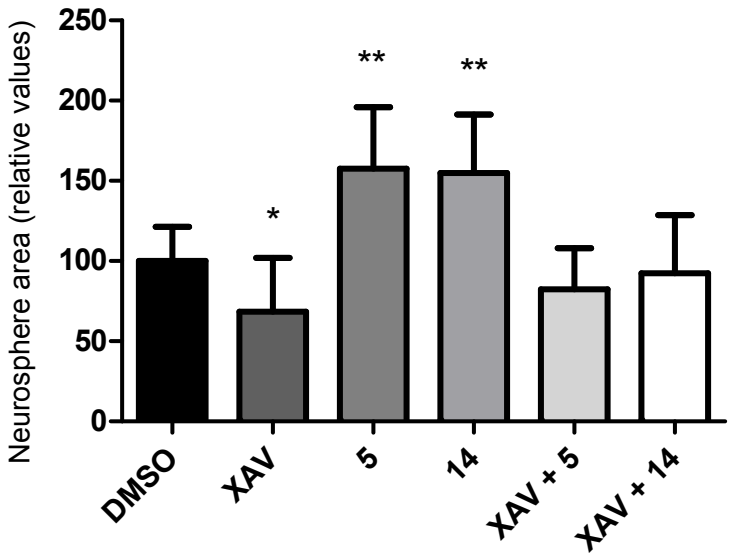

Figure 11. LRKK2 inhibitors promote proliferation of NSCs and progenitors through the activation of Wnt canonical pathway. Quantitative analysis of total neurosphere area after 4 days in culture in the presence of DMSO as a control, 1 μM XAV393 Wnt signaling inhibitor (XAV), 1 μM LRRK2 inhibitors **5** or **14**, or the

combination of both, as indicated. The total neurosphere area was measured in each field using an especially designed macro for IMAGE J. Results are mean values ± standard error of the mean (SEM), represented as relatives to control value (=100), of 6 different fields each one from triplicates and from three independent experiments. Student's test comparing each treatment with that of DMSO; *$p \leq 0.05$; **$p \leq 0.005$. Neurospheres were prepared from 2 female mice

Next, we analyzed whether the most promising LRRK2 inhibitors (**5** and **14**) together with the control reference PF-475 could regulate neural cell differentiation after adhesion of dissociated cells from SVZ neurospheres to a poly-ornithine//fibronectin coverslide.[49] Neurospheres were cultured for 6 days with the compounds at a concentration of 1μM without mitogens. On the 7th day cells were fixed and immuno-stained using β3-tubulin as a neuronal marker, CNPase as an oligodendrocytic marker, GFAP for astrocytes and bisbenzimide for nuclei. Images were taken by confocal microscopy and the number of positive cells for each marker was counted. Treatment with LRRK2 inhibitors increased significantly the number of differentiated CNPase positive oligodendrocytes, whereas in the case of neurons, although there was a constant tendency to increase the number of positive β3-tubulin cells compared to control, the compound treatment did not reached statistical significance (Figure 12). Regarding the number of GFAP positive cells, it remained constant despite treatment with the LRRK2 inhibitors (data not shown).

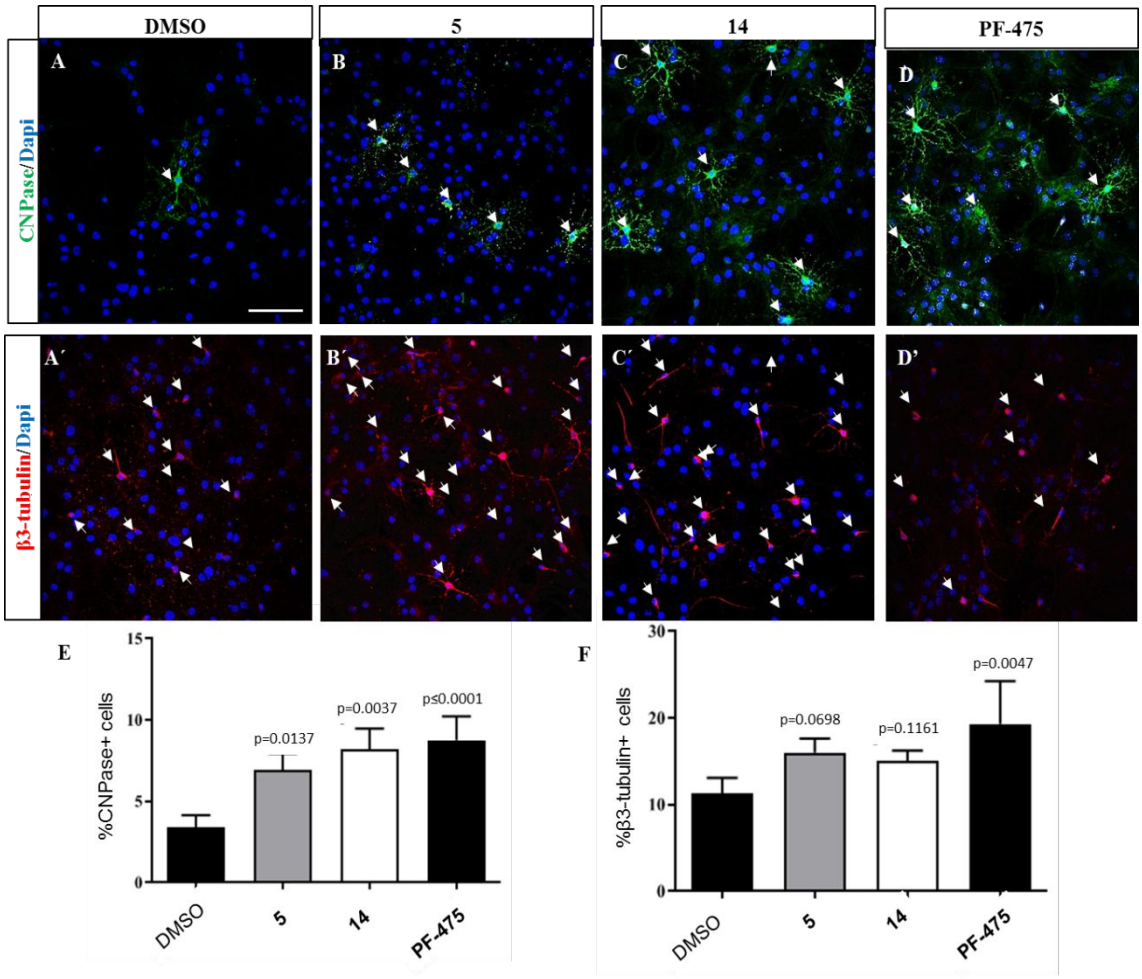

Figure 12. Analysis of neuronal differentiation in NSCs and progenitors from V-SVZ adult brain grown in the presence of LRRK2 inhibitors. Dissociated cells from adult SVZ neurospheres grown for 7 days without mitogens in the presence of control (DMSO) **(A, A')**, benzothiazole derivative **5 (B, B'), 14 (C, C')** and the control **PF-475 (D,D')**. Representative immunofluorescent field micrographs showing the different neural cell types generated: oligodendrocytes expressing CNPase (green) and neurons expressing β3-tubulin (red). The nuclei are stained with bisbenzimide (blue) in all the panels. **(E, F)** Quantification analysis of the differentiated cells in culture. Results are mean value ± SEM, represented as relatives to total number of cells (=100), of 4 different fields each one from triplicates and from two independent experiments. Bar in A: 50 µm. Neurospheres were prepared separately in three experiments from a total number of four mice (2 females and 2 males).

These results suggest that benzothiazole-based LRRK2 inhibitors have the potential to drive differentiation of neural stem cells mostly toward an oligodendrocytic fate, opening new fields for future therapeutic application.

Target engagement and kinase profiling

Finally, in order to confirm that this oligodendrocytic and neurogenic potential was indeed driven by LRRK2 inhibition, we performed target engagement experiments with the adult V-SVZ neurospheres. Two LRRK2 auto-phosphorylation sites have been used as a measurement of LRRK2 activity: Ser935 and Ser1292. However, some authors report that Ser935 is not a direct LRRK2 auto-phosphorylation site.[50] Furthermore, one report that compared LRRK2 Ser935 and Ser1292 phosphorylation showed that the same LRRK2 inhibitor affected differently at these epitopes.[48] Recent experiments show that a possible better way of measuring LRRK2 activity and thus, LRRK2 inhibitor engagement is by measuring its downstream substrate, the phosphorylation of Rab10.[51-52] For this reason, we quantified the amount of phosphorylated Rab10 in neurospheres cultures when the cells are treated with the selected benzothiazole-based LRRK2 inhibitors by Western blotting. These experiments showed that in three different replicates the phosphorylation of Rab10 was decreased as result of LRRK2 catalytic activity being inhibited when the cells were treated with LRRK2 inhibitors **5** and **14** at a dose of 10μM compared to control (Figure 13).

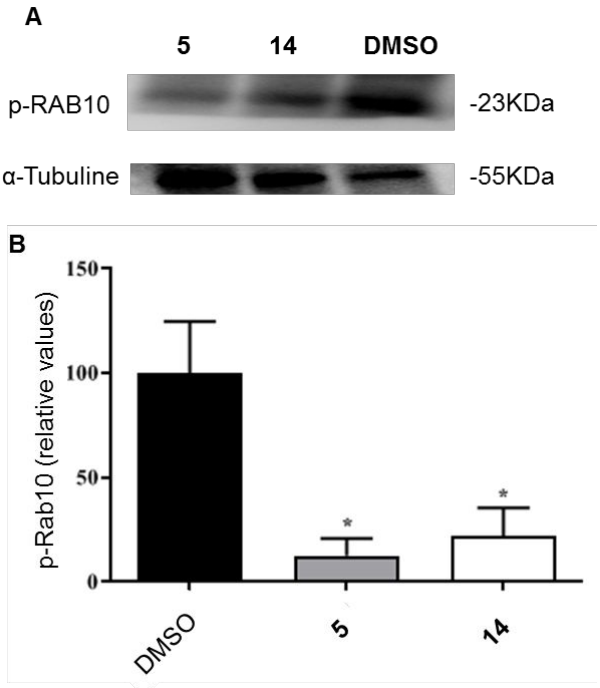

Figure 13. (A) LRRK2 inhibitor treatment reduces Rab10 phosphorylation. Neurosphere cultures grown for 7 days in the presence of mitogens were treated either with DMSO (control) or with the LRRK2 inhibitors **5** and **14**. Cell pellets were obtained as described in the experimental section. The levels of p-Rab10 were analysed by immunoblotting using a monoclonal antibody to p-Rab10 (T73) in three different experiments. **(B)** Quantification analysis. Results are mean value ± SEM of the three experiments. *$p<0.05$. Neurospheres were prepared from 2 male mice.

Finally, since the catalytic domain of protein kinases is highly conserved along the kinome, selectivity of one of the active benzothiazole-based LRRK2 inhibitors here studied (compound **5**) was determined. The percentage of protein kinase activity at a fixed dose of 10 μM for compound **5** was calculated on a panel of 50 different protein kinases including tyrosine and serine/threonine kinases. Moreover, CK-1δ and CK-1ε were specifically included based in the benzothiazole central scaffold which is also present in others potent CK-1 inhibitors.[53-54] Compound **5** shows a good selectivity with a final selectivity score or "S" score, a quantitative measure of compound selectivity calculated by dividing the number of kinases that compounds bind to by the total number of distinct kinases tested, excluding mutant variants,[55] of 0.02 as it only

interacts with 1 out of 50 kinases evaluated with a percentage of activity below 35% (Figure 14).

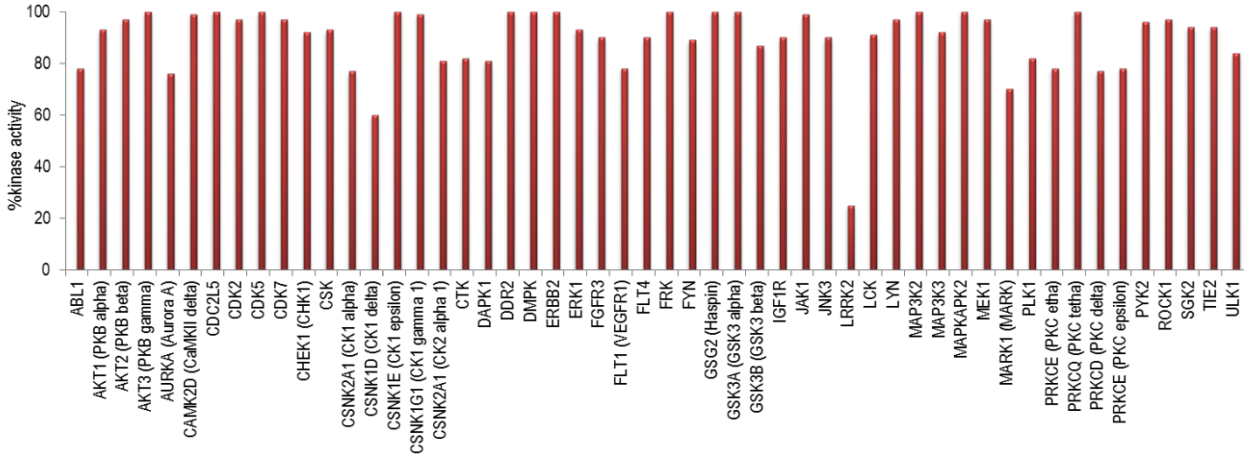

Figure 14. Protein kinase profile for benzothiazole-based LRRK2 inhibitor **5**.

Conclusions

In this work a new family of LRRK2 inhibitors, based on the benzothiazole scaffold, have been synthesized. In addition, their inhibitory activity was determined and a potential binding mode of these new molecules and the SAR were studied using a homology LRRK2 model. The ability of all the active compounds to penetrate the BBB was predicted using the *in vitro* PAMPA assay. Those compounds that were predicted to be BBB penetrant were used as pharmacological tools to determine if the pharmacological inhibition of LRRK2 could promote adult neurogenesis. This was first performed using an HTS assay to determine if the LRRK2-inhibitors modulated Wnt signaling in the presence of Wnt3a protein with the selected compounds then further evaluated to determine their dose dependency. The most promising inhibitors, compounds **5, 10, 14** and **19**, were then evaluated in a proliferation assay of neurospheres prepared from the SVZ of adult mice. Using the size of the neurosphere measured as total area of the sphere as a read out of proliferation, it was found that

LRRK2 inhibition by chemically diverse inhibitors promoted the proliferation of NSCs and neural progenitors. In relation to this aspect, the proliferating activity of two selected LRRK2 inhibitors, benzothiazoles **5** and **14**, was exerted, at least in part, by enhancing Wnt signaling pathway. Moreover, LRRK2 inhibitors **5** and **14**, promoted oligodendrogliogenesis and a tendency toward neurogenesis. Lastly, in order to confirm that this effect was indeed dependent on LRRK2 inhibition, target engagement experiments were performed by quantification of the decrease in a Rab10 phosphorylation, a known substrate of LRRK2.

Taken together, our findings shown that the pharmacological inhibition of LRRK2 with the benzothiazole-based inhibitors has the potential to activate Wnt-signaling, promote the proliferation of NSCs and neural progenitors and drive the differentiation towards neuronal and oligodendrocytic cell fates. This is of crucial importance in the neurodegeneration field as these inhibitors may act as multifunctional drugs. The fact that LRRK2 inhibitors are able to promote the differentiation towards oligodendrocytes opens a new avenue for the application of these inhibitors in multiple sclerosis or other demyelinating diseases in which oligodendrocyte cell-death is one of the features of the pathology.

Experimental section

Chemistry. Substrates were purchased from commercial sources (Sigma Aldrich, Acros, Fluorochem and TCI-Europe) and used without further purification. The microwave equipment used was an Initiator TM from Biotage®. Crude residues were purified with the indicated solvent as eluent by column chromatography carried out at medium pressure using silica gel (E. Merck, Grade 60, particle size 0.040 – 0.063 mm, 230 – 240 mesh ASTM) or by IsoleraOne flash purification system from Biotage® using columns SF10-4g Si 50 AX1368-8 from Agilent Technologies and KP-Sil 10 from Biotage®. Thin Layer Chromatography was done in chromatographic sheets (Merck type 60 F254 with a width of 0.2 mm). Compounds were detected with UV light (254 nm). ^{1}H-NMR spectra were obtained on the Bruker AVANCE-300 spectrometer from the CAI-UCM working at 300 MHz. Typical spectral parameters: spectral width 16 ppm, pulse width 9 μs (57°), data size 32 K. ^{13}C-NMR experiments were carried out on the Bruker AVANCE-300 spectrometer operating at 75 MHz or on a Bruker AV 500 MHz spectrometer working at 125 MHz from the CAI-UCM. The acquisition parameters: spectral width 16 kHz, acquisition time 0.99 s, pulse width 9 μs (57°), data size 32 K. Chemical shifts are reported in values (ppm) relative to internal Me_4Si and *J* values are reported in Hz. The multiplicity of the signals (s: singlet, d: doublet, dd: doublet of doublets, t: triplet, td: triplet of doblets, q: quadruplet, qt: quintuplet, m: multiplet), the coupling constants (*J*) and the specific characterization of each compound are shown. HPLC analyses were performed on Alliance Waters 2690 equipment, with a UV detector photodiode array Waters 2996 with MS detector MicromassZQ (Waters), using an Sunfire column C18, 3.5 μm (50 mm × 4.6 mm) and acetonitrile and MilliQ water (with 0.1% formic acid) as mobile phase or in an HPLC-

MS equipment form Thermo Fisher coupled to a Finnigan TM LXQ TM detector using an Sunfire column C18, 3.5 μm (50 mm × 4.6 mm) and acetonitrile and MilliQ water (with 0.1% formic acid) as mobile phase. The standard gradient consisted of a 10 min run from 15% to 95% of acetonitrile at a flow rate of 1 $mL \cdot min^{-1}$. Melting points were determined with a Buchi M560 apparatus. High resolution mass spectrometry (HRMS) was done in a spectrometer LC/MSD 100 Hewlett Packard using positive Electro Spray techniques (ESI). Values are expressed in mass units (m/z). Elemental analyses were performed by the analytical department at CENQUIOR (CSIC) and CAI-UCM, and the results obtained were within ± 0.4% of the theoretical values using the analyzer Heraeus CHN-O-rapid. All the final compounds have a purity ≥95% tested by HPLC.

(Benzoxazol-2-yl)-4-morpholinobenzamide (3). 2-Aminobenzoxazole (64.0 mg, 0.3 mmol) were dissolved in anhydrous tetrahydrofuran under N_2 atmosphere in a bath with acetone and dry ice (-78 ºC). After 5 minutes, *1H*-benzo[*d*][1,2,3]triazol-1-yl 4-morpholinobenzoate (100.0 mg, 0.3 mmol) dissolved in anhydrous tetrahydrofuran (330 μL) of nBuLi solution (1.4 M in hexane) were added onto the first solution. The mixture was stirred for 1 hour, and then the crude was washed with a saturated NaCl solution. Afterwards, the solvent was removed under reduced pressure and the remaining solid was purified by flash column chromatography using CH_2Cl_2/MeOH (20:1) as eluents, to afford the desired product as a white solid (63.0 mg, 63%) M.p.: 220.0 - 222.0 ºC. ^{1}H-NMR (300 MHz, $CDCl_3$): δ 8.14 - 7.93 (m, 2 H), 7.46 - 7.34 (d, *J* = 5.6 Hz, 1 H), 7.29 - 7.08 (m, 3 H), 6.81 (d, *J* = 8.8 Hz, 2 H), 3.83 - 3.71 (m, 4 H), 3.29 - 3.12 (m, 4 H). ^{13}C-NMR (75 MHz, $CDCl_3$) δ 162.5, 154.2, 130.6, 124.9, 123.9, 113.6, 113.5, 110.6, 66.6, 47.7. Purity HPLC: 99%. MS (ESI+): *m/z* 324 $[M+H]^+$. Anal. ($C_{18}H_{17}N_3O_3$) Calculated: C 66.86%, H 5.30%, N 13.00%. Found: C 66.60%, H 5.55%, N 13.22%.

***N*-(Benzimidazol-2-yl)-4-morpholinobenzamide (4).** 4-Morpholinobenzoic acid (311.0 mg, 1.5 mmol), EDCI (374.0 mg, 2.0 mmol), DMAP (36.0 mg, 0.3 mmol) and triethylamine (335 μL, 2.4 mmol) were dissolved in anhydrous CH_2Cl_2. After stirring the mixture during 1 hour at r.t., 2-aminobenzimidazole (200.0 mg, 1.5 mmol) were added. The resulting mixture was stirred overnight at r.t. Afterwards, the crude was washed with saturated $NaHCO_3$ and saturated NaCl solutions. The solvent of the organic phase was then removed under reduced pressure and the remaining solid was purified by flash column chromatography using CH_2Cl_2/MeOH (20:1) as eluents to afford the desired product as a white solid (156.0 mg, 36%) M.p.: 221.0 - 223.0 ºC. ^{1}H-NMR (300 MHz, $CDCl_3$): δ 7.71 (d, *J* = 8.8 Hz, 2 H), 7.38 (d, *J* = 7.8 Hz, 1 H), 7.14 (t, *J* = 7.7 Hz, 1 H), 6.90 (d, *J* = 8.9 Hz, 2 H), 6.88 - 6.75 (m, 1 H), 6.60 (d, *J* = 8.0 Hz, 1 H), 5.99 (s, 1 H), 4.01 - 3.78 (m, 4 H), 3.51 - 3.13 (m, 4 H). ^{13}C-NMR (75 MHz, $CDCl_3$): δ 169.2, 154.6, 154.4, 142.3, 132.0, 131.8, 123.9, 122.1, 120.12, 116.8, 113.1, 113.0, 66.5, 47.2. Purity HPLC: 96%. MS (ESI+): *m/z* 323 $[M+H]^+$. Anal. ($C_{18}H_{18}N_4O_2$) Calculated: C 67.07%, H 5.63%, N 17.38%. Found: C 66.89%, H 5.45%, N 17.60%.

***N*-(Benzothiazol-2-yl)-4-morpholinobenzamide (5).** 4-Morpholinobenzoic acid (276.0 mg, 1.3 mmol), EDC (331.0 mg, 1.3 mmol) and DMAP (33.0 mg, 0.3 mmol) were dissolved in anhydrous CH_2Cl_2. After stirring the mixture during 1 hour at r.t., 2-aminobenzothiazole (200.0 mg, 1.3 mmol) were added. The resulting mixture was stirred overnight at r.t. Afterwards, the crude was washed with saturated $NaHCO_3$ and saturated NaCl solutions. The solvent of the organic phase was then removed under reduced pressure and the remaining solid was purified by flash column chromatography using CH_2Cl_2/MeOH (20:1) as eluents to afford the desired product as a white solid (72.0 mg, 18%). M.p.: 237.6 - 240.0 ºC. ^{1}H-NMR (300 MHz, $CDCl_3$) δ 10.21 (s, 1 H, NH), 7.90 (d, *J* = 9.0 Hz, 2 H), 7.84 (dd, *J* = 8.5, 1.5 Hz, 1 H), 7.62 (dd, *J* = 8.3, 1.2 Hz,

1 H), 7.44 - 7.35 (m, 1 H), 7.35 - 7.27 (m, 1 H), 4.01 - 3.71 (m, 4 H), 3.49 - 3.16 (m, 4 H). ^{13}C-NMR (75 MHz, DMSO-d_6) δ 164.6, 159.1, 154.3, 148.2, 132.2, 129.4, 126.0, 123.7, 121.3, 121.1, 120.7, 113.8, 66.5, 47.4. Purity HPLC: 97%. MS (ESI+): *m/z* 340 $[M+H]^+$. Anal. ($C_{18}H_{17}N_3O_2S$) Calculated: C 63.70%, H 5.05%, N 12.38%, S 9.45%. Found: C 63.58%, H 4.98%, N 12.40%, S 9.31%.

General procedure for the synthesis of *N*-(benzothiazole-2-yl)-aryl-amide derivatives 5-23: The synthesis was performed by a coupling reaction between the corresponding 2-amino-benzothiazole and the corresponding aromatic acid. Each 2-amino-benzothiazole was mixed with the aromatic acid in CH_2Cl_2 or THF (specified for each case) at the specific temperature and time detailed for each compound and in the presence of the corresponding coupling agent and the corresponding basic catalyst. Previously, the aromatic acid was activated with the coupling agent and the basic catalyst for a certain time and temperature and then the corresponding 2-amino-benzothiazole was added. After the indicated time, the reaction mixture was washed with different inorganic solutions, detailed in each case. Finally, the organic phase was dried over magnesium sulfate and the solvent was evaporated under reduced pressure. The crude was purified as indicated for each compound obtaining the desired product as a solid.

***N*-(6-Methoxybenzothiazol-2-yl)-4-morpholinobenzamide (6).** Reagents: 4-morpholinobenzoic acid (230.0 mg, 1.1 mmol), EDCI (276.6 mg, 1.4 mmol), DMAP (24.4 mg, 0.2 mmol), triethylamine (248 μL, 1.8 mmol) and 2-amino-6-methoxybenzothiazole (200.0 mg, 1.1 mmol) dissolved in CH_2Cl_2. Activation reaction: 1 hour at r.t. Coupling reaction: overnight at r.t. Work-up: washes with saturated $NaHCO_3$ and saturated NaCl solutions. Purification: column chromatography using CH_2Cl_2/MeOH (50:1) as eluents. Yield: 36.0 mg, 9%, yellow solid. M.p.: 237.6 - 240.0

ºC. ^{1}H-NMR (300 MHz, $CDCl_3$) δ 9.47 (s, 1H), 7.88 (d, *J* = 9.0 Hz, 2H), 7.64 (d, *J* = 8.8 Hz, 1H), 7.33 (d, *J* = 2.6 Hz, 1H), 7.04 (dd, *J* = 8.8, 2.6 Hz, 1H), 6.94 (d, *J* = 9.0 Hz, 2H), 3.93 - 3.83 (m, 7H), 3.36 - 3.31 (m, 4H). ^{13}C-NMR (75 MHz, DMSO-d_6) δ 164.8, 156.9, 156.0, 153.8, 142.7, 132.8, 129.8, 120.8, 120.5, 114.8, 113.1, 104.6, 65.8, 55.6, 46.8. Purity HPLC: 95%. MS (ESI+): *m/z* 370 $[M+H]^+$. HRMS (ESI+) ($C_{19}H_{19}N_3O_3S$) $[M+H]^+$: Calculated: 370.12199, Found: 370.12218.

***N*-(6-Trifluoromethylbenzothiazol-2-yl)-4-morpholinobenzamide (7)**. Reagents: 4-morpholinobenzoic acid (189.9 mg, 0.9 mmol), EDCI (228.5 mg, 1.4 mmol), DMAP (22.4 mg, 0.2 mmol), triethylamine (223 µL, 1.8 mmol) and 2-amino-6-trifluoromethylbenzothiazole (200.0 mg, 0.9 mmol) dissolved in CH_2Cl_2. Activation reaction: 1 hour at r.t. Coupling reaction: overnight at r.t. Work-up: washes with saturated $NaHCO_3$ and saturated NaCl solutions. Purification: column chromatography using Hex/AcOEt (50:1) as eluents. Yield: 79.0 mg, 26%, yellow solid. M.p.: 218.5 - 218.5 ºC. ^{1}H-NMR (300 MHz, $CDCl_3$) δ 8.14 (s, 1H), 7.96 (d, *J* = 8.9 Hz, 2H), 7.73 - 7.57 (m, 2H), 6.89 (d, *J* = 8.9 Hz, 2H), 3.92 - 3.81 (m, 4H), 3.36 - 3.27 (m, 4H). ^{13}C-NMR (125 MHz, $CDCl_3$) δ 163.8, 160.8, 153.5, 149.4, 131.2, 128.6, 124.9 (q, J_{C-F} = 32.5 Hz), 123.3 (q, J_{C-F} = 272.1 Hz), 122.1 (q, J_{C-F} = 3.4 Hz) 119.8, 119.6, 118.04 (q, J_{C-F} = 4.4 Hz), 112.7, 65.4, 46.3. Purity HPLC: >99%. MS (ESI+): *m/z* 408 $[M+H]^+$. HRMS (ESI+) ($C_{19}H_{17}FN_3O_2S$) $[M+H]^+$: Calculated: 408.09881, Found: 408.09965. Anal. ($C_{19}H_{16}F_3N_3O_2S$) Calculated: C 56.01%, H 3.96%, N 10.31%, S 7.87%. Found: C 56.13%, H 3.98%, N 10.38%, S 7.59%.

***N*-(6-Methylbenzothiazol-2-yl)-4-morpholinobenzamide (8).** Reagents: 4-morpholinobenzoic acid (252.4 mg, 1.2 mmol), EDCI (303.5 mg, 1.6 mmol), DMAP (20.1 mg, 0.2 mmol), triethylamine (272 µL, 1.9 mmol) and 2-amino-6-methylbenzothiazole (200.0 mg, 0.9 mmol) dissolved in CH_2Cl_2. Activation reaction: 6

hours at r.t. Coupling reaction: overnight at r.t. Work-up: washes with HCl (0.1 M), saturated $NaHCO_3$ and saturated NaCl solutions. Purification: automatic chromatographic system (Biotage®Isolera One) using Hex/AcOEt as eluents. Yield: 43.0 mg, 10%, yellow solid. M. p.: 287.7 - 288.8 ºC. ^{1}H-NMR (300 MHz, $CDCl_3$) δ 10.56 (s, 1H), 7.89 (d, *J* = 8.9 Hz, 2H), 7.63 (s, 1H), 7.42 (d, *J* = 8.3 Hz, 1H), 7.16 (dd, *J* = 8.3, 1.7 Hz, 1H), 6.85 (d, *J* = 8.9 Hz, 2H), 3.87 - 3.83 (m, 4H), 3.29 - 3.26 (m, 4H), 2.46 (s, 3H). ^{13}C-NMR (75 MHz, $CDCl_3$) δ 164.7, 158.5, 154.2, 146.1, 133.7, 132.3, 129.4, 127.5, 121.3, 121.1, 120.3, 113.8, 66.5, 47.5, 21.4. Anal. ($C_{19}H_{19}N_3O_2S$) Calculated: C 64.57%, H 5.42%, N 11.89%, S 9.07%. Found: C 64.33%, H 5.38%, N 11.85%, S 8.96%.

***N*-(6-Chlorobenzothiazol-2-yl)-4-morpholinobenzamide (9).** Reagents: 4-morpholinobenzoic acid (224.4 mg, 1.1 mmol), EDCI (269.9 mg, 1.4 mmol), DMAP (26.4 mg, 0.2 mmol), triethylamine (242 μL, 1.7 mmol) and 2-amino-6-chlorobenzothiazole (200.0 mg, 1.1 mmol) dissolved in CH_2Cl_2. Activation reaction: 1 hour at r.t. Coupling reaction: overnight at r.t. Work-up: washes with HCl (0.1 M), saturated $NaHCO_3$ and saturated NaCl solutions. Purification: automatic chromatographic system (Biotage®Isolera One) using Hex/AcOEt as eluents. Yield: 96.0 mg, 24%, white solid. M.p.: 245.4 - 246.4 ºC. ^{1}H-NMR (300 MHz, $CDCl_3$) δ 10.25 (s, 1H), 7.89 (d, *J* = 8.9 Hz, 2H), 7.81 (d, *J* = 2.1 Hz, 1H), 7.52 (d, *J* = 8.7 Hz, 1H), 7.33 (dd, *J* = 8.7, 2.1 Hz, 1H), 6.89 (d, *J* = 9.0 Hz, 2H), 3.92 - 3.82 (m, 4H), 3.33 - 3.30 (m, 4H). ^{13}C-NMR (75 MHz, $CDCl_3$) δ 164.5, 159.3, 154.4, 146.9, 133.5, 129.4, 126.7, 121.5, 121.0, 120.8, 113.7, 107.0, 66.5, 47.4. Purity HPLC: >99%. MS (ESI+): *m/z* 374 $[M+H]^+$. HRMS (ESI+) ($C_{18}H_{17}ClN_3O_2S$) $[M+H]^+$: Calculated: 374.07245, Found: 374.07161. Anal. ($C_{18}H_{16}ClN_3O_2S$) Calculated: C 57.83%, H 4.31%, N 11.24%, S 8.58%. Found: C 57.56%, H 4.09%, N 11.43%, S 8.40%.

***N*-(6-Fluorobenzothiazol-2-yl)-4-morpholinobenzamide (10).** Reagents: 4-morpholinobenzoic acid (168.2 mg, 1.2 mmol), EDCI (296.3 mg, 1.5 mmol), DMAP (29.1 mg, 0.2 mmol), triethylamine (265 μL, 1.9 mmol) and 2-amino-6-fluorobenzothiazole (200.0 mg, 1.2 mmol) dissolved in CH_2Cl_2. Activation reaction: 1 hour at r.t. Coupling reaction: overnight at r.t. Work-up: washes with HCl (0.1 M), saturated $NaHCO_3$ and saturated NaCl solutions. Purification: automatic chromatographic system (Biotage®Isolera One) using Hex/AcOEt as eluents. Yield: 79.0 mg, 19%, white solid. M.p.: 228.3 - 229.3 ºC. ^{1}H-NMR (300 MHz, $CDCl_3$) 7.90 (d, J = 8.9 Hz, 2H), 7.54 (dd, J = 8.9, 4.6 Hz, 1H), 7.48 (dd, J = 7.9, 2.6 Hz, 1H), 7.10 (td, J = 7.9, 2.6 Hz, 1H), 6.85 (d, J = 8.9 Hz, 2H), 3.87 - 3.85 (m, 4H), 3.34 - 3.30 (m, 4H). ^{13}C-NMR (125 MHz, $CDCl_3$) δ 165.4, 160.0 (d, J_{C-F} = 243.5 Hz), 159.9, 154.7, 144.8, 133.4 (d, J_{C-F} = 10.5 Hz), 130.0, 121.9 (d, J_{C-F} = 9.0 Hz), 121.4, 114.7 (d, J_{C-F} = 24.5 Hz), 114.1, 108.0 (d, J_{C-F} =26.5 Hz), 66.9, 47.8. Purity HPLC: 97.3%. MS (ESI+): *m/z* 358 $[M+H]^+$. HRMS (ESI+) ($C_{18}H_{17}FN_3O_2S$) $[M+H]^+$: Calculated: 358.10200, Found: 358.10317. Anal. ($C_{18}H_{16}FN_3O_2S$) Calculated: C 60.49%, H 4.51%, N 11.76%, S 8.97%. Found: C 60.68%, H 4.50%, N 11.55%, S 8.72%.

***N*-(4-Methylbenzothiazol-2-yl)-4-morpholinobenzamide (11).** Reagents: 4-morpholinobenzoic acid (252.4 mg, 1.2 mmol), EDCI (303.5 mg, 1.6 mmol), DMAP (24.6 mg, 0.2 mmol), triethylamine (272 μL, 1.9 mmol) and 2-amino-4-methylbenzothiazole (200.0 mg, 1.2 mmol) dissolved in CH_2Cl_2. Activation reaction: 1 hour at r.t. Coupling reaction: overnight at r.t. Work-up: washes with HCl (0.1 M), saturated $NaHCO_3$ and saturated NaCl solutions. Purification: automatic chromatographic system (Biotage®Isolera One) using Hex/AcOEt as eluents. Yield: 93.0 mg, 45%, white solid. M.p.: 289 - 290 ºC. ^{1}H-NMR (300 MHz, $CDCl_3$) δ 10.29 (s, 1H), 7.93 (d, J = 9.0 Hz, 2H), 7.74 (d, J = 7.9 Hz, 1H), 7.47 (d, J = 7.9 Hz, 1H), 7.25 (t,

J = 7.9 Hz, 1H) 6.94 (d, *J* = 9.0 Hz, 2H), 3.90 - 3.86 (m, 4H), 3.36 - 3.33 (m, 4H), 2.64 (s, 3H). ^{13}C-NMR (75 MHz, $CDCl_3$) δ 164.3, 157.8, 154.2, 147.5, 132.0, 130.4, 129.2, 126.8, 123.8, 121.2, 118.8, 113.7, 66.5, 47.4, 18.1. Purity HPLC: >99%. MS (ESI+): *m/z* 354 $[M+H]^+$. HRMS (ESI+) ($C_{19}H_{19}N_3O_2S$) $[M+H]^+$: Calculated: 354.12707, Found: 354.12705.

***N*-(4-Chlorobenzothiazol-2-yl)-4-morpholinobenzamide (12).** Reagents: 4-morpholinobenzoic acid (224.5 mg, 1.1 mmol), EDCI (269.9 mg, 1.5 mmol), DMAP (24.5 mg, 0.2 mmol), triethylamine (272 μL, 1.9 mmol) and 2-amino-4-chlorobenzothiazole (200.0 mg, 1.2 mmol) dissolved in CH_2Cl_2. Activation reaction: 1 hour at r.t. Coupling reaction: overnight at r.t. Work-up: washes with HCl (0.1 M), saturated $NaHCO_3$ and saturated NaCl solutions. Purification: automatic chromatographic system (Biotage®Isolera One) using Hex/AcOEt as eluents. Yield: 29.0 mg, 5%, white solid. M.p.: 148.5 - 150 ºC. ^{1}H-NMR (300 MHz, $CDCl_3$) δ 7.98 (d, *J* = 9.0 Hz, 2H), 7.75 (dd, *J* = 7.9, 1.0 Hz, 1H), 7.49 (dd, *J* = 7.9, 1.0 Hz, 1H), 7.29 (t, *J* = 7.9 Hz, 1H), 6.95 (d, *J* = 9.0 Hz, 2H), 3.92 - 3.82 (m, 4H), 3.40 - 3.30 (m, 4H). ^{13}C-NMR (75 MHz, $CDCl_3$) δ 163.3, 158.6, 153.4, 144.0, 132.3, 128.4, 125.5, 124.0, 123.5, 119.4, 119.0, 112.8, 65.5, 46.4. Purity HPLC: >99%. MS (ESI+): *m/z* 374 $[M+H]^+$. Anal. ($C_{18}H_{16}ClN_3O_2S$) Calculated: C 57.83%, H 4.31%, N 11.24%, S 8.58%. Found: C 57.44%, H 4.78%, N 10.84%, S 8.04%. HRMS (ESI+) ($C_{18}H_{16}ClN_3O_2S$) $[M+H]^+$: Calculated: 374.07300, Found: 374.07315.

***N*-(6-Ethoxybenzothiazol-2-yl)-4-morpholinobenzamide (13).** Reagents: 4-morpholinobenzoic acid (213.1 mg, 1.0 mmol), EDCI (256.2 mg, 1.3 mmol), DMAP (25.1 mg, 0.2 mmol), triethylamine (272 μL, 1.9 mmol) and 2-amino-6-ethoxybenzothiazole (200.0 mg, 1.0 mmol) dissolved in CH_2Cl_2. Activation reaction: 6 hours at r.t. Coupling reaction: overnight at r.t. Work-up: washes with HCl (0.1 M),

saturated $NaHCO_3$ and saturated NaCl solutions. Purification: automatic chromatographic system (Biotage®Isolera One) using Hex/AcOEt as eluents. Yield: 20.0 mg, 5%, white solid. M.p.: 222.8 - 223.8 ºC. ^{1}H-NMR (300 MHz, $CDCl_3$) δ 7.95 (d, *J* = 8.9 Hz, 2H), 7.49 (d, *J* = 8.9 Hz, 1H), 7.30 (d, *J* = 2.4 Hz, 1H), 7.04 (dd, *J* = 8.9, 2.4 Hz, 1H), 6.89 (d, *J* = 8.9 Hz, 2H), 4.09 (q, *J* = 6.9 Hz, 2H), 3.89 - 3.69 (m, 4H), 3.38 - 3.25 (m, 4H), 1.43 (t, *J* = 6.9 Hz, 3H). ^{13}C-NMR (75 MHz, $CDCl_3$) δ 163.4, 157.1, 155.3, 153.3, 139.1, 131.4, 128.6, 119.7, 119.5, 114.9, 112.7, 104.1, 65.5, 63.2, 46.4, 13.8. Purity HPLC: 95%. MS (ESI+): *m/z* 384 $[M+H]^+$. Anal. ($C_{20}H_{21}N_3O_3S$) Calculated C 62.64%, H 5.52%, N 10.96%, S 8.36%. Found C 62.25%, H 5.53%, N 10.56%, S 8.09%.

***N*-(6-Bromobenzothiazol-2-yl)-4-morpholinobenzamide (14)**. Reagents: 4-morpholinobenzoic acid (180.9 mg, 0.9 mmol), EDCI (217.56 mg, 1.1 mmol), DMAP (21.3 mg, 0.2 mmol), triethylamine (195 μL, 0.9 mmol) and 2-amino-6-bromobenzothiazole (200.0 mg, 1.0 mmol) dissolved in CH_2Cl_2. Activation reaction: 6 hours at r.t. Coupling reaction: overnight at r.t. Work-up: washes with HCl (0.1 M), saturated $NaHCO_3$ and saturated NaCl solutions. Purification: automatic chromatographic system (Biotage®Isolera One) using Hex/AcOEt as eluents. Yield: 41.0 mg, 11%, white solid. M.p.: 237.5 - 238.5 ºC. ^{1}H-NMR (300 MHz, $CDCl_3$) δ 10.51 (s, 1H), 7.96 (d, *J* = 1.6 Hz, 1H), 7.87 (d, *J* = 9.0 Hz, 2H), 7.44 (dd, *J* = 8.6, 1.6 Hz, 1H), 7.38 (d, *J* = 8.6 Hz, 1H), 6.86 (d, *J* = 9.0 Hz, 2H), 3.89 - 3.83 (m, 4H), 3.33 - 3.26 (m, 4H). ^{13}C-NMR (125 MHz, $CDCl_3$) δ 165.2, 160.8, 154.9, 145.7, 133.5, 130.3, 129.9, 124.5, 121.6, 120.7, 117.5, 114.1, 66.9, 47.8. Purity HPLC: >99%. MS (ESI+): *m/z* 418 [M+2]. HRMS (ESI+) ($C_{18}H_{16}BrN_3O_2S$) $[M+H]^+$: Calculated: 420.02919, Found: 420.02075.

***N*-(6-Ethylcarboxylatebenzothiazol-2-yl)-4-morpholinobenzamide (15).** Reagents: 4-morpholinobenzoic acid (279.7 mg, 1.3 mmol), PyBOP (1.5 g, 2.5 mmol), HOBt (350 mg, 2.8 mmol), triethylamine (780 µL, 5.6 mmol) and 2-amino-6-(ethylcarboxylate)benzothiazole (200.0 mg, 1.2 mmol) dissolved in THF. Activation reaction: 1 hour under microwave irradiation at 50 ºC. Coupling reaction: 5 hours under microwave irradiation at 110 ºC. Work-up: wash with HCl (0.1 M). Purification: recrystallization from CH_2Cl_2/^{i}Pr-OH (99:1). Yield: 50.0 mg, 11%, white solid. M.p: 250.3 - 250.8 ºC. ^{1}H-NMR (300 MHz, $CDCl_3$) δ 10.44 (s, 1H), 8.56 (d, *J* = 1.4 Hz, 1H), 8.06 (dd, *J* = 8.5, 1.4 Hz, 1H), 7.90 (d, *J* = 9.0 Hz, 2H), 7.58 (d, *J* = 8.5 Hz, 1H), 6.88 (d, *J* = 9.0 Hz, 2H), 4.42 (q, *J* = 7.1 Hz, 2H) 3.90 - 3.81 (m, 4H), 3.34 - 3.27 (m, 4H), 1.43 (t, *J* = 7.1 Hz, 3H). ^{13}C-NMR (75 MHz, $CDCl_3$) δ 165.2, 163.8, 161.1, 150.5, 131.1, 128.5, 126.5, 124.9, 122.5, 119.7, 119.2, 112.7, 65.5, 60.1, 46.4, 13.4. Purity HPLC: >98% MS (ESI+): *m/z* 412 $[M+H]^+$. Anal. ($C_{21}H_{21}N_3O_4S$) Calculated: C 61.30%, H 5.14%, N 10.21%, S 7.79%. Found: C 60.96%, H 5.25%, N 9.86%, S 7.53%.

***N*-(6-Propoxybenzothiazol-2-yl)-4-morpholinobenzamide (16).** Reagents: 4-morpholinobenzoic acid (248.8 mg, 1.2 mmol), EDCI (299.0 mg, 1.6 mmol), DMAP (30.0 mg, 0.2 mmol), triethylamine (267 µL, 0.9 mmol) and 2-amino-6-propoxybenzothiazole (200.0 mg, 1.0 mmol) dissolved in CH_2Cl_2. Activation reaction: 6 hours at r.t. Coupling reaction: overnight at r.t. Work-up: washes with HCl (0.1 M), saturated $NaHCO_3$ and saturated NaCl solutions. Purification: automatic chromatographic system (Biotage®Isolera One) using CH_2Cl_2/MeOH as eluents. Yield: 127.0 mg, 27%, white solid. M.p.: 232.1 - 232.7 ºC. ^{1}H-NMR (300 MHz, $CDCl_3$) δ 10.29 (s, 1H), 7.88 (d, *J* = 9.0 Hz, 1H), 7.46 (d, *J* = 8.9 Hz, 1H), 7.31 (d, *J* = 2.5 Hz, 1H), 6.96 (dd, *J* = 8.9, 2.5 Hz, 1H), 6.88 (d, *J* = 9.0 Hz, 1H), 3.98 (t, *J* = 6.6 Hz, 2H), 3.89 - 3.83 (m, 4H), 3.32 - 3.27 (m, 4H), 1.85 (m, 1H), 1.06 (t, *J* = 7.4 Hz, 2H). ^{13}C-

NMR (75 MHz, $CDCl_3$) δ 163.6, 156.3, 155.2, 153.3, 141.3, 132.3, 128.4, 120.4, 120.3, 114.5, 112.8, 103.9, 69.2, 65.5, 46.5, 21.6, 9.5. Purity HPLC: >95%. MS (ESI+): *m/z* 398.25 $[M+H]^+$. HRMS (ESI+) ($C_{19}H_{23}N_3O_3S$) $[M+H]^+$: Calculated: 398.15329, Found: 398.15275.

***N*-(6-Isopropylbenzothiazol-2-yl)-4-morpholinobenzamide (17).** Reagents: 4-morpholinobenzoic acid (269.4 mg, 1.7 mmol), EDCI (324.0 mg, 1.7 mmol), DMAP (32.0 mg, 0.3 mmol), triethylamine (290 μL, 1.9 mmol) and 2-amino-6-isopropylbenzothiazole (250.0 mg, 1.3 mmol) dissolved in CH_2Cl_2. Activation reaction: 6 hours at r.t. Coupling reaction: overnight at r.t. Work-up: washes with HCl (0.1 M), saturated $NaHCO_3$ and saturated NaCl solutions. Purification: automatic chromatographic system (Biotage®Isolera One) using CH_2Cl_2/MeOH as eluents. Yield: 218.4 mg, 44%, white solid. M.p.: 238.2 - 238 ºC. ^{1}H-NMR (300 MHz, $CDCl_3$) δ 10.35 (s, 1H), 7.89 (d, *J* = 9.0 Hz, 2H), 7.68 (d, *J* = 1.7 Hz, 1H), 7.49 (d, *J* = 8.3 Hz, 1H), 7.26 - 7.22 (m, 1H), 6.85 (d, *J* = 9.0 Hz, 2H), 3.89 - 3.81 (m, 4H), 3.33 - 3.25 (m, 4H), 3.03 (m, 1H), 1.31 (d, *J* = 6.9 Hz, 6H). ^{13}C-NMR (75 MHz, $CDCl_3$) δ 163.7, 157.7, 153.2, 145.3, 143.9, 131.3, 128.4, 124.0, 120.4, 119.4, 117.5, 112.8, 65.5, 46.5, 33.2, 23.3. Purity HPLC: 95%. MS (ESI+): *m/z* 382.25 $[M+H]^+$. HRMS (ESI+) ($C_{19}H_{23}N_3O_2S$) $[M+H]^+$: Calculated: 382.15837, Found: 382.15932.

***N*-(6-Methylsulfonylbenzothiazol-2-yl)-4-morpholinobenzamide (18).** Reagents: 4-morpholinobenzoic acid (227.0 mg, 1.1 mmol), EDCI (274.1 mg, 1.4 mmol), DMAP (37.0 mg, 0.2 mmol), triethylamine (245 μL, 1.8 mmol) and 2-amino-6-methyl-sulfonylbenzothiazole (250.0 mg, 1.1 mmol) dissolved in CH_2Cl_2. Activation reaction: 6 hours at r.t. Coupling reaction: overnight at r.t. Work-up: washes with HCl (0.1 M), saturated $NaHCO_3$ and saturated NaCl solutions. Purification: column chromatography using Hex/AcOEt (1:9) as eluents. Yield: 50.0 mg, 18%, white solid. M.p.: 299.7 - 300

ºC. ^{1}H-NMR (300 MHz, DMSO-d_6) δ 12.86 (s, 1H), 8.66 (s, 1H), 8.09 (d, J = 8.9 Hz, 2H), 7.97 - 7.91 (m, 2H), 7.06 (d, J = 8.9 Hz, 2H), 3.78 - 3.71 (m, 4H), 3.36 - 3.29 (s, 4H), 3.26 (s, 3H). ^{13}C-NMR (125 MHz, DMSO-d_6) δ 163.0, 154.0, 149.5, 144.6, 140.1, 135.2, 130.1, 124.7, 121.9, 120.4, 114.4, 113.1, 65.8, 46.7, 44.0. Purity HPLC: 95%. MS (ESI+): *m/z* 418.13 $[M+H]^+$. HRMS (ESI+) ($C_{19}H_{23}N_3O_4S$) $[M+H]^+$: Calculated: 418.08897, Found: 418.08802.

***N*-(6-Fluorobenzothiazol-2-yl)-benzamide (19).** Reagents: benzoic acid (145.3 mg, 1.2 mmol), EDCI (296.3 mg, 1.1 mmol), DMAP (29.3 mg, 0.2 mmol), triethylamine (265 µL, 1.9 mmol) and 2-amino-6-fluorobenzothiazole (200.0 mg, 1.2 mmol) dissolved in CH_2Cl_2. Activation reaction: 6 hours at r.t. Coupling reaction: overnight at r.t. Work-up: washes with HCl (0.1 M), saturated $NaHCO_3$ and saturated NaCl solutions. Purification: automatic chromatographic system (Biotage®Isolera One) using Hex/AcOEt as eluents Yield: 90.0 mg, 28%, white solid. M.p.: 262.8 - 264 ºC. ^{1}H-NMR (300 MHz, DMSO-d_6) δ 12.91 (s, 1H), 8.12 (d, J = 8.6 Hz, 2H), 7.93 (dd, J = 8.7, 2.8 Hz, 1H), 7.79 (dd, J = 8.7, 2.7 Hz, 1H), 7.66 (t, J = 8.5, 2H), 7.56 (t, J = 8.5 Hz, 2H), 7.31 (td, J = 8.5, 4.8 Hz, 1H). ^{13}C-NMR (75 MHz, DMSO-d_6) δ 165.9, 158.8, 158.7 (d, $J_{C\text{-}F}$ = 234.7 Hz), 155.7, 145.3 (d, $J_{C\text{-}F}$ = 18.2 Hz) 132.9, 131.7, 128.6, 128.3, 121.5, 114.3 (d, J = 24.5 Hz), 108.1 (d, J = 26.9 Hz). Purity HPLC: >99%. MS (ESI+): *m/z* 273 $[M+H]^+$. HRMS (ESI+) ($C_{14}H_9FN_2OS$) $[M+H]^+$: Calculated: 273.04924 Found: 273.04788.

***N*-(6-Fluorobenzothiazol-2-yl)-4-chlorobenzamide (20).** Reagents: 4-chlorobenzoic acid (146.2 mg, 1.2 mmol), EDCI (296.3 mg, 1.1 mmol), DMAP (29.3 mg, 0.2 mmol), triethylamine (265 µL, 1.9 mmol) and 2-amino-6-fluorobenzothiazole (200.0 mg, 1.2 mmol) dissolved in CH_2Cl_2. Activation reaction: 6 hours at r.t. Coupling reaction: overnight at r.t. Work-up: washes with HCl (0.1 M), saturated $NaHCO_3$ and saturated

NaCl solutions. Purification: automatic chromatographic system (Biotage®Isolera One) using Hex/AcOEt as eluents. Yield: 25.0 mg, 28%, white solid. M.p.: 262.8 - 264 ºC. ^{1}H-NMR (300 MHz, DMSO-d_6) δ 13.00 (s, 1H), 8.15 (d, J = 8.6 Hz, 2H), 7.95 (dd, J = 8.7, 2.8 Hz, 1H), 7.86 - 7.74 (m, 1H), 7.56 (d, J = 8.5 Hz, 2H), 7.31 (td, J = 8.5, 4.8 Hz, 1H). ^{13}C NMR (75 MHz, DMSO-d_6) δ 165.9, 158.8, 158.7 (d, J_{C-F} = 240.7 Hz), 154.6, 145.2 (d, J_{C-F} = 13.8 Hz) 132.9, 131.7, 128.6, 128.3, 121.5, 114.3 (d, J_{C-F} = 24.6 Hz), 108.2 (d, J_{C-F} = 26.9 Hz). Purity HPLC: >99%. MS (ESI+): *m/z* 307 $[M+H]^+$. HRMS (ESI+) ($C_{14}H_8FClN_2OS$) $[M+H]^+$: Calculated: 307.01027, Found: 307.01053.

***N*-(6-Fluorobenzothiazol-2-yl)-5-(p-tolyl)furan-2-carboxamide (21).** Reagents: 5-(*p*-tolyl)furan-2-carboxylic acid (300.6 mg, 1.5 mmol), PyBOP (296.3 mg, 1.1 mmol), DMAP (29.3 mg, 0.2 mmol), triethylamine (265 μL, 1.9 mmol) and 2-amino-6-fluorobenzothiazole (200.0 mg, 1.2 mmol) dissolved in CH_2Cl_2. Activation reaction: 6 hours at r.t. Coupling reaction: overnight at r.t. Work-up: washes with HCl (0.1 M), saturated $NaHCO_3$ and saturated NaCl solutions. Purification: automatic chromatographic system (Biotage®Isolera One) using Hex/AcOEt as eluents Yield: 25.0 mg, 28%, white solid. M.p: 245.1 - 245.7 ºC ^{1}H-NMR (300 MHz, $CDCl_3$) δ 7.67 (dd, J = 8.9, 4.6 Hz, 1H), 7.57 (d, J = 8.2 Hz, 2H), 7.51 (dd, J = 8.9, 2.6 Hz, 1H), 7.48 (d, J = 3.7 Hz, 1H), 7.23 (d, J = 8.2 Hz, 2H), 7.13 (td, J = 8.9, 2.6 Hz, 1H), 6.79 (d, J = 3.7 Hz, 1H), 2.40 (s, 3H). ^{13}C-NMR (75 MHz, $CDCl_3$) δ 164.9, 158.6 (d, J_{C-F} = 243.7 Hz) 156.9, 156.3, 154.4, 143.1, 138.7, 132.3 (d, J_{C-F} = 10.7 Hz), 128.6, 125.1, 123.8, 120.7 (d, J_{C-F} = 9.4 Hz), 119.2, 113.6 (d, J_{C-F} = 24.6 Hz), 106.6 (d, J_{C-F} = 26.1 Hz), 20.4. Purity HPLC: >99%. MS (ESI+): *m/z* 353$[M+H]^+$. HRMS (ESI+) ($C_{19}H_{13}FN_2O_2S$) $[M+H]^+$: Calculated: 353.07545, Found: 353.07641.

***N*-(6-Fluorobenzothiazol-2-yl)-6-methoxy-2-naphthamide (22).** Reagents: 6-methoxy-2-naphtoic acid (201.2 mg, 1.8 mmol), PyBOP (1.9 g, 3.7 mmol), HOBt (502.0 mg, 3.7 mmol), triethylamine (1.04 mL, 7.4 mmol) and 2-amino-6-fluorobenzothiazole (250.0 mg, 1.5 mmol) dissolved in CH_2Cl_2. Activation reaction: 1 hour at r.t. Coupling reaction: overnight at r.t. Work-up: wash with HCl (0.1 M) solution. Purification: recrystallization from: CH_2Cl_2:^{i}Pr-OH (99:1). Yield: 36.5 mg, 7%, white solid. M.p,: 248.5 - 248.8 ºC. ^{1}H-NMR (300 MHz, DMSO-d_6) δ 12.94 (s, 1H), 8.76 (d, J = 1.8 Hz, 1H), 8.12 (dd, J = 8.9, 1.9 Hz, 1H), 8.03 - 7.91 (m, 3H), 7.80 (dd, J = 8.9, 4.8 Hz, 1H), 7.45 - 7.43 (m, 1H), 7.35 - 7.26 (m, 2H), 3.92 (s, 3H). ^{13}C-NMR (125 MHz, DMSO-d_6) δ 159.6, 159.3, 158.7 (d, $J_{C\text{-}F}$ = 240.0 Hz), 145.3, 136.6, 132.8 (d, $J_{C\text{-}F}$ = 8.7 Hz), 130.9, 129.4, 129.1, 127.3, 127.0, 126.5, 124.8, 121.5, 119.7, 114.2 (d, $J_{C\text{-}F}$ = 24.5 Hz), 108.1 (d, $J_{C\text{-}F}$ = 26.8 Hz), 105.9, 55.4. Purity HPLC: >99%. MS (ESI+): *m/z* 353[M+H]$^+$. HRMS (ESI+) ($C_{19}H_{13}FN_2O_2S$) [M+H]$^+$: Calculated: 353.07545, Found: 353.07641.

***N*-(6-Fluorobenzothiazol-2-yl)-5-oxo-5-phenylpentamide (23).** Reagents: 5-oxo-5-phenylpentanoic acid (342.7 mg, 1.8 mmol), PyBOP (1.9 g, 3.7 mmol), HOBt (502.0 mg, 3.7 mmol), triethylamine (1.04 mL, 7.4 mmol) and 2-amino-6-fluorobenzothiazole (250.0 mg, 1.5 mmol) dissolved in CH_2Cl_2. Activation reaction: 1 hour at r.t. Coupling reaction: overnight at r.t. Work-up: wash with HCl (0.1 M) solution. Purification: recrystallization from: CH_2Cl_2/^{i}Pr-OH (99:1). Yield: 200.0 mg, 48%, white solid. M.p.: 212.4 - 213.1 ºC. ^{1}H-NMR (300 MHz, DMSO-d_6) δ 12.38 (s, 1H), 8.00 - 7.95 (m, 2H), 7.88 (dd, J = 8.7, 2.7 Hz, 1H), 7.73 (dd, J = 8.9, 4.8 Hz, 1H), 7.67 - 7.60 (m, 1H), 7.55 - 7.50 (m, 2H), 7.27 (td, J = 9.1, 2.7 Hz, 1H), 3.12 (t, J = 7.1 Hz, 2H), 2.59 (t, J = 7.4 Hz, 2H), 1.98 (qt, J = 7.2 Hz, 2H). ^{13}C-NMR (125 MHz, DMSO-d_6) δ 199.8, 172.43, 158.9 (d, $J_{C\text{-}F}$ = 239.7 Hz), 158.2, 145.5, 136.9, 133.5, 133.0 (d, $J_{C\text{-}F}$ = 11.1 Hz), 129.0, 128.2,

121.9 (d, $J_{C\text{-}F}$ = 9.17 Hz), 114.4 (d, $J_{C\text{-}F}$ = 24.5 Hz) 108.4 (d, $J_{C\text{-}F}$ = 26.9 Hz), 48.9, 37.4, 34.6. Purity HPLC: >99%. MS (ESI+): *m/z* 343 $[M+H]^+$. Anal. ($C_{18}H_{15}FN_2O_2S$) Calculated %C: 63.14, %H: 4.42, %N: 8.18, %S: 9.36. Found: %C: 62.93, %H: 4.40, %N: 8.26, %S: 9.38.

Computational studies

Docking studies. As target structure, the LRRK2 homology model based on previous publication[34] was here used. The structure was then prepared using Protein Preparation Wizard[56] implemented on Maestro.[57] Hydrogen atoms were added. The protein was ionized at pH=7.2, refined carrying out H-bond assignment and restrain minimization using OPLS2005 force field.[58] Ligands were built using the 2D Sketcher module implemented in Maestro and prepare for the docking process using LigPrep.[59] LigPrep builds a 3D-structure for each ligand, ionizing them at pH = 7.2 ± 0.2, searching for one lower energy ring conformation for the aliphatic rings and calculating atomic charges using OPLS2005. A rigid-receptor docking study was carried out using Glide[60] in the extra precision (XP) mode. The grid for the following docking process was centered on the centroid of the residues Lys1906 and Glu1920. For this docking study, OPLS2005 force field was used and a maximum number of 50 poses per ligand were reported. The best energetically ranked poses for each ligand were analyzed visually.

Biology

***In vitro* LRRK2 and LRRK2 G2019S activity assay.** $LRRK2_{wt}$ and LRRK2-G2019S kinase activity was measured externally using Adapta® Screen technology from Life Technologies™ (Invitrogen) consisting of a fluorescent-based immunoassay for the detection of ADP.[35]Kinase activity was evaluated following the Adapta assay validation

protocols PV4873 and PV4881 for LRRK2 and LRRK2 G2019S respectively. Duplicate assay mixtures were set up each in a 10 µL volume containing 17 ng (8 nM) of recombinantly expressed, human LRRK2 protein (Cat. ♯PV4873), 200 µM LRRKtide (Cat. ♯PV5093), 25 mM Tris / 7.5 mM HEPES pH 8.2, 5 mM $MgCl_2$, 0.5 mM EGTA, 10 µM ATP, 0.01% NaN_3, 0.005% Brij-35, 1% DMSO and compound of interest in a series of concentrations (e.g. for 10 point titrations, 3-fold serial dilutions are conducted starting from 100 µM concentration) in a 384 well microplate (Corning model 3674). Mutant LRRK2 G2019S inhibition was determined similarly except that due to the higher specific activity 0.5 ng (2.5 nM) of the LRRK2 G2019S mutant kinase (Cat. ♯ PV4881) is used in the assays. A series of controls were incubated on the same plate with: (i) kinase inactivated by EDTA, and (ii) mixtures containing incrementally increased ADP concentrations from 0 to 100 µM, and inversely decreased ATP concentrations from 100 to 0 µM, to establish a standard curve delimited by ADP concentrations corresponding to no conversion and complete conversion of ATP in the assay mixture. After 1h incubation at ambient temperature, 5 µL of the Adapta® Assay Detection Mix (Cat. ♯ PV5099) was added, containing 30 mM EDTA to stop the kinase reaction, 6 nM of the Eu-labelled anti-ADP antibody (Cat.♯ (PV5097), and 18.9 nM of the AlexaFluor°-ADP conjugate (Cat.♯ PV5098). The plate was allowed to equilibrate at room temperature for at least 30 minutes before being read out in a fluorescence microplate reader to establish the ratio of emissions at 665 nm (ADP-tracer) and at 615 nm (Eu-antibody) as a measure of ADP concentration by virtue of Fluorescence Resonance Energy Transfer (FRET). The conversion in % of ATP into ADP by the kinase reaction in each well is determined from the ADP/ATP standard curve, and means are formed from each duplicate assay well. The resultant mean conversion ratios for the kinase assays containing increasing concentrations of inhibitor are fitted to a

sigmoidal binding model (Graphpad), with the assay containing no inhibitor (<40% ATP conversion for linearity) taken as the 100% activity control (top), and the control assay with the kinase inhibited by excess EDTA as the 0% activity control (bottom). The IC_{50} is determined by the intersection of the fitted curve (dose-response sigmoidal fitting) with the 50% activity. The fitting was performed using Origin 9.0 software. Values and standard deviations were calculated from ten different concentrations per compound in two independent experiments. Kinase profiling was determined externally using the Kinome$_{scan}$™ methodology from DiscoverX.[61]

CNS Penetration: *in vitro* parallel artificial membrane permeability assay (PAMPA). Prediction of the brain penetration was evaluated using the PAMPA methodology. Ten commercial drugs (Sigma, Acros organics, Merck, Aldrich and Fluka), dodecane (Sigma) and porcine polar brain lipid (PBL) (Avanti Polar Lipids) were purchased. The donor plate used was a 96-well filtrate plate (Multiscreen®) and the acceptor plate was an indented 96-well plate (Multiscreen®). Filter PDVF membrane units (Symta) were used to filtered the samples. A 96-well plate UV reader (Thermoscientific, Multiskan spectrum) was used for the UV measurements. Test compounds: caffeine, enoxacine, hydrocortisone, desipramine, ofloxacine, piroxicam, testosterone, promazine, verapamile and atenolol were weighted and dissolved in EtOH to a final concentration of 100 µM. 100 µL of this compound stock solution was taken and 1400 µL of EtOH and 3500 µL of PBS (pH = 7.4) were added to reach 30% of EtOH concentration in the experiment. These solutions were then filtered. The acceptor 96-well microplate was filled with 180 µL of PBS:EtOH (7:3). The donor 96-well plate was coated with 4 µL of porcine brain lipid in dodecane (20 mg·mL^{-1}) and after 5 minutes, 180 µL of each compound solution was added to the donor 96-well plate. Then the donor plate was carefully put on the acceptor plate to form a “sandwich”, which was

left undisturbed for 2 h and 30 min at 25 °C. During this time the compounds diffused from the donor plate through the brain lipid membrane into the acceptor plate. After that time, the donor plate was removed. UV plate reader determined the concentration of compounds and commercial drugs in the acceptor and the donor wells. Every sample was analyzed at three to five wavelengths, in triplicates and in two independent runs. Results are given as the mean of the two runs ± SD. Ten quality control compounds (previously mentioned) of known BBB permeability were included in each experiment to validate the analysis set.

Real time RT-PCR for LRRK2 and AXIN2 expression in NPCs. Culturing human iPSC-NPCs was performed as previously described.[41] 6-well plates were used in this assay. Plates were prepared with polyornithine/laminin coating. Polyornithine (Sigma) was dissolved in distilled water to a final concentration of 10 $mg \cdot mL^{-1}$ and was finally diluted 1:500 and dispensing it in each well. The polyornithine solution was left on the glass slides at least for 2 hours at r.t. Laminin (Sigma) was dissolved in PBS at a $1mg \cdot mL^{-1}$ and finally diluted 1:200 to be dispensed into the wells prior to removing the polyornithine solution. The plates were then left with the laminin solution overnight at the incubator. Before cell seeding, coating reagent was removed through a wash with NPC media (350 mL DMEM (Gibco), 150 mL Hams-F12 (MediaTech), 5 mL of 100X penicillin/streptomycin and 10 mL of B27 (Thermo Fisher). Single-cell suspensions in NPC media were prepared from the human iPSC-NPCs 8330-8 cell line and dispensed into 6-well plates at the seeding density of 2000000 cells per well. After confluency RNA was isolated from the cells using the Direct-zol™ RNA Kit (Zymo Research). The concentration of total RNA was measured using a NanoDrop and cDNA was synthesized using the cDNA Kit (Zymo Research). Real time PCR reactions were performed in the Roche 480 Light Cycler in a 384-well plate. Into each well was added

5µL of TaqMan 2X Gene Expression Master Mix (Thermo Fisher 4369510), 0.5µL of 20X commercial TaqMan primer probe (Thermo Fisher, *LRRK2*: Hs01115057_m1, *AXIN2:* Hs00610344_m1, *GAPDH*: Hs02786624_g1), 0.5µL of DNase/RNase-free H_2O, and 5µL of above diluted cDNA.. Cycle threshold (Ct) values were obtained automatically from the Roche 480 Light Cycler software. Results were normalized to *GAPDH* expression. Values represent the mean fold change to control values (iPSC in the case of *LRRK2* expression and DMSO for *AXIN2* expression) from triplicates. Quantitative analyses were carried out in three separate experiments, calculating the mean ± SEM and using a two-tailed Student's *t*-test to determine statistically relevant changes.

Wnt modulation assay. Derivation of human iPSC-NPCs, culturing human iPSC-NPCs, creation of the TCF/LEF reporter line, and the production of NPC-compatible Wnt3a-conditioned media was performed as previously described.[41] White 384-well microplates were used in this assay. Plates were prepared with the polyornithine/laminin coating procedure described above with robotic handling, including aspiration with a Power Washer PW384 (Tecan) and dispensing with a Matrix WellMate microplate dispenser (Thermo Scientific), to provide standardized operation. For 384-well plates, 20 µL of coating reagents were used. A quick spin step was included after dispensing of each coating reagent and later cell suspension for 384-well plates to ensure that all liquid was brought down to the bottom of wells. Before cell seeding, coating reagent was removed through a wash with NPC media (previously described[41]). For these experiments, single-cell suspensions in NPC media were prepared from the human iPSC-NPCs, stably integrated with the TCF/LEF luciferase reporter, and dispensed into 384-well plates at the seeding density of 6000 cells per well, using a Matrix WellMate (Thermo Scientific) microplate dispenser. The next day, cells were treated for 24 hours

with 10% Wnt-conditioned media (prepared previously from mouse L cells) and the LRRK2 inhibitors at 1 μM and 10 μM using a CyBio liquid handling system (CyBio®). Just prior to the luminescence reading, the plates were taken out of a 37 °C incubator and equilibrated to room temperature for 30 min before the SteadyGlo reagent (Promega) was dispensed (volume equal 1:1 SteadyGlo:culture medium). Luminescence was measured after a 10 min incubation using an EnVision multilabel plate reader (PerkinElmer). For the single-dose experiments values represent the mean of triplicates of one experiment. For the dose-dependent experiments the same protocol was followed but in this case concentrations of 0.01, 0.03, 0.10, 0.30, 0.93, 2.70, 8.30 and 20 μM of the selected LRRK2 inhibitors were used. Values represent the mean ± SEM of eight repetitions of three independent experiments.

Immunohistochemistry of LRRK2 in the SVZ of adult mice. All animal care and handling were carried out in accordance with European Union guidelines (directives 86/609/EEC and 2010/63/EU) and Spanish legislation (Law 32/2007 and RD 53/2013), and the protocols were approved by the Ethical Committee of the Consejo Superior de Investigaciones Cientificas (CSIC) and Comunidad de Madrid (Ref. PROEX 078/17). All efforts were made to ameliorate the suffering of the animals and to reduce the number of animals used to a minimum. Two males and one female male 2.5 months old mice of the C57/Bl6 strain from the repository of Institute Cajal were perfused intracardially with 4% paraformaldehyde (PFA) and their brain was post-fixed, cryoprotected, frozen and then serial coronal cryostat sections (15 μM) were obtained. The sections were first blocked in 0.2 - 0.3% Triton X-100, 10% Normal Goat Serum (NGS) dissolved in PBS and they were then incubated for 24 - 72 hours with the following primary antibodies: Anti-DCX (Goat, 1:3000, Santa Cruz, sc-8066), Anti-GFAP (mouse, 1:1000, N206A/8), Anti-SOX2 (goat, 1:1000, R&D AF2018) and Anti-

LRRK2 (rabbit, 1:1000, Millipore ABN187). The sections were then washed with PBS and followed with incubation for 1 hour at r.t. with the following secondary antibodies: anti-goat-Alexa647, anti-mouse-Alexa488 and anti-rabbit-Alexa-594. (all at 1:1000 from Invitrogen).Bisbenzimide (1:1000, Sigma) was used to stain the nuclei. Afterwards, the sections were mounted in Fluromont-G solution (SouthernBiotech). Images were obtained using confocal microscopy (Leica TCSP5and LASX software. At least three sections from each animal were analyzed.

Neurosphere cultures and proliferation assays. Neurosphere (NS) cultures were derived from the subventricular zone of 6 young adult mice (6 weeks old; 2 males and 4 females of the strain C57/Bl6 from the repository of Institute Cajal) and induced to proliferate using established passaging methods to achieve optimal cellular expansion according to published protocols.[62] Briefly, mice were euthanized with CO_2, brains were removed and the subventricular zone was dissected, cut up into pieces and digested using 0.7 $mg \cdot mL^{-1}$ papain (Sigma), 0.2 $mg \cdot mL^{-1}$ cysteine (Sigma) and 0.2 $mg \cdot mL^{-1}$ EDTA (Sigma) before it was gently disaggregated. The resulted cell suspension was plated into 8 wells of a 12-wells plates containing DMEM-F12 (Gibco) supplemented with 10 $mg \cdot mL^{-1}$ of N2 (Thermo Fisher), and B27 (Thermo Fisher). The cells were passaged by mechanical procedures and were maintained until passage 3 for the first experiments, with alternative daily addition of both 10 $ng \cdot mL^{-1}$ of FGF (Peprotech) and 2 $ng \cdot mL^{-1}$ of EGF (Peprotech). Cell proliferation assays were performed on floating neurospheres in 96-well plates at a density of 5000 cells per cm^2. LRRK2 inhibitors or Wnt signalling inhibitor XAV393 (Sigma) were diluted in DMSO at a concentration of 10 mM and then added to the dissociated cells to a final concentration of 1 μM or 5 μM of each alone or in combination and 0.1% DMSO was used as a control. Each treatment was repeated by triplicate and the cells were left to grow at 37 ˚C and 5% of CO_2 in an

incubator for 4 days. On the fourth day, for the measurement of the size and number of the neurospheres, photographs were taken by bright field microscopy (Leica DMI 6000) using an automatic pattern, taken 6 pictures of different areas of each well with the 10X objective. The total number and area of neurospheres bigger than 400 μm^2 cell area was measured using a macro software for Image J, (National Institute of Health) designed at the Cajal Institute. Quantitative analyses were carried out in three separate experiments, calculating the mean ± SEM and using a two-tailed Student's *t*-test to determine statistically relevant changes.

Differentiation experiments. For the differentiation experiments, cells were initially expanded as neurospheres, then cultured on polyornithine and fibronectin (Sigma) coated glass coverslips in DMEM/F12 (Gibco) supplemented with B27 (Thermo Fisher) for 7 days in the absence of mitogens (density at plating: 100000 cells per cm^2), 0.1% DMSO as a control or the indicated LRRK2 inhibitor at 10 μM was added to the media. Cells were then fixed with 4% PFA and immunostained. Immunocytochemistry**:** the differentiated cells adhered to glass coverslips were washed with PBS, and then permeabilized with 0.1% Triton X-100 for 1 hour at r. t. Cells were incubated overnight at 4 ˚C with the corresponding primary antibodies: Anti-β-III-tubulin (chicken, 1:1000, Abcam ab41489), Anti-CNPase (mouse, 1:300, BioLegend 836401), Anti-GFAP (rabbit, 1:2000, DAKO Z0334).The cells were then washed with PBS and incubated for 1 hour at r.t. with the following secondary antibodies: anti-chicken IgG-Alexa-555, anti-mouse IgG-Alexa-488, anti-rabbit IgG-Alexa-647 (all at 1:1000, from Invitrogen) and Bisbenzimide (1:1000, Sigma). The coverslips were then mounted with Fluromont-G solution (SouthernBiotech). Images were obtained using confocal microscopy (Leica TCSP5). Quantification was undertaken with LASX software. The results are expressed as the mean value of triplicates of the percentage of positive cells compared to total

number of cells ± SEM of three biological independent experiments and using a two-tailed Student's *t*-test to determine statistically relevant changes.

p-Rab 10 Western Blot experiments. Neurosphere cultures were derived from the subventricular zone of 2 young male adult C57BL/6 mice (6 weeks old; from the repository of Institute Cajal). Neurospheres suspension was plated into p100 plates at a density of 5000 cells/cm^2 containing DMEM-F12 (Gibco) supplemented with 10 mg·mL^{-1} of N2 (Thermo Fisher), and B27 (Thermo Fisher) and with alternative daily addition of both 10 ng·mL^{-1} of FGF (Peprotech) and 2 ng·mL^{-1} of EGF (Peprotech) and the corresponding LRRK2 inhibitors at a dose of 10μM. The neurospheres were cultured for 7 days. On the last day neurospheres were collected in PBS, lysed in RIPA buffer (Boston Bio-Products) supplemented with protease inhibitors (Roche Complete Mini tablets), and phosphatase inhibitors (Sigma), followed by centrifugation at 20,000G for 15 min. Supernatants were transferred to new tubes and total protein concentration was quantified with the Pierce BCA Protein Assay Kit (Thermo Fisher). WB lots were performed by running 10 μg of total protein (pre-boiled for 5 min in loading buffer (Invitrogen) at 95ºC) on 10% pre-cast SDS-polycrilamide gels (Biorad). The proteins were then transferred onto PVDF membranes (EMD Millipore) using standard procedures. Membranes were blocked in 5% BSA (Biorad) in Tris-buffered saline with Tween-20 (Biorad) for 1 hour, incubated overnight with the corresponding primary antibodies at 4°C: p-Rab 10 (T73) (rabbit, 1:1000, abcam) and α-tubulin (1:1000) as loading control. Followed by the corresponding secondary antibodies incubation (Biorad), and lastly incubated with SuperSignal West Pico Chemiluminescent Substrate (Thermo Fisher) according to manufacturer's instructions. Membranes were then exposed for different amounts of time, to account for bands of different intensities (and to ensure detection of all relevant bands). Films were scanned

using a GS-800 Calibrated Densitometer (Biorad), and band intensities were quantified using Image J, (National Institute of Health). Relative intensity was calculated relative to the respective loading control (tubulin band).

Supporting information

The Supporting Information is available free of charge on the ACS Publications website.

Experimental permeability data in the PAMPA-BBB assay for commercial drugs used in the experiment validation; linear correlation between experimental and reported permeability of commercial drugs using the PAMPA-BBB assay; HPLC chromatograms for compounds **3-23** (PDF)

Molecular formula strings and some data (CSV)

Corresponding authors information:

*A.M.: e-mail, ana.martinez@csic.es.

*A.V.M.: e-mail, aixamorales@cajal.csic.es.

ORCID

Ana Martinez: 0000-0002-2707-8110

Aixa V. Morales: 0000-0001-6295-5142

Carmen Gil: 0000-0002-3882-6081

Notes:

The authors declare no competing financial interest

Acknowledgements

We are grateful for the technical help of Maria Ciorraga in neurosphere cultures and Carmen Hernández from Image Analysis Unit at Cajal Institute with ImageJ macro design. This work was supported by MINECO (grant SAF2016-76693-R to A.M. and

SAF2017-85717-R to A.V.M.), CIBERNED (CB18/05/00040 to A.M.), MECD (FPU13-003262 to J.Z.-D.), CEU-Banco Santander (Scholarships for the Research Mobility Program CEU-BANCO SANTANDER to J.Z.-D.), Fundación Alicia Koplowitz (Research Project, 2018 to A.V.M.) and Tau Consortium and Stuart & Suzanne Steele MGH Research Scholar Award to S.J.H.

Abbreviations used

ADP, adenosine diphosphate; BBB, blood brain barrier; CNS, central nervous system; Dcx, doublecortain; DMAP, 4-dimethylaminopyridine; EDCI, 1-ethyl-3-(3-dimethylaminopropyl)carbodiimide; GSK-3, glycogen synthase kinase 3; GTP, guanosine triphosphate; HOBt, hydroxybenzotriazole; LRRK2, leucine repeat rich kinase; NPC, neural progenitor cell; PD, Parkinson's disease; PyBOP, benzotriazol-1-yl-oxytripyrrolidinophosphonium hexafluorophosphate; SAR, structure activity relationship; TCF/LEF, T-cell factor/lymphoid enhancer-binding factor; V-SVZ, ventricular-subventricular zone;

References

(1) Gunosewoyo, H.; Yu, L.; Munoz, L.; Kassiou, M. Kinase targets in CNS drug discovery. *Future Med Chem* **2017,** *9*, 303-314.

(2) Chan, S. L.; Tan, E. K. Targeting LRRK2 in Parkinson's disease: an update on recent developments. *Expert Opin Ther Targets* **2017,** *21*, 601-610.

(3) West, A. B. Achieving neuroprotection with LRRK2 kinase inhibitors in Parkinson disease. *Exp Neurol* **2017,** *298*, 236-245.

(4) Li, J. Q.; Tan, L.; Yu, J. T. The role of the LRRK2 gene in parkinsonism. *Mol Neurodegener* **2014,** *9*, 47.

(5) Marin, I. Ancient origin of the Parkinson disease gene LRRK2. *J Mol Evol* **2008,** *67*, 41-50.

(6) Cardona, F.; Tormos-Perez, M.; Perez-Tur, J. Structural and functional in silico analysis of LRRK2 missense substitutions. *Mol Biol Rep* **2014,** *41*, 2529-2542.

(7) Mata, I. F.; Wedemeyer, W. J.; Farrer, M. J.; Taylor, J. P.; Gallo, K. A. LRRK2 in Parkinson's disease: protein domains and functional insights. *Trends Neurosci* **2006,** *29*, 286-293.

(8) Anand, V. S.; Braithwaite, S. P. LRRK2 in Parkinson's disease: biochemical functions. *FEBS J* **2009,** *276*, 6428-6435.

(9) Steger, M.; Tonelli, F.; Ito, G.; Davies, P.; Trost, M.; Vetter, M.; Wachter, S.; Lorentzen, E.; Duddy, G.; Wilson, S.; Baptista, M. A.; Fiske, B. K.; Fell, M. J.; Morrow, J. A.; Reith, A. D.; Alessi, D. R.; Mann, M. Phosphoproteomics reveals that Parkinson's disease kinase LRRK2 regulates a subset of Rab GTPases. *Elife* **2016,** *5*, 1-28.

(10) Kanao, T.; Venderova, K.; Park, D. S.; Unterman, T.; Lu, B.; Imai, Y. Activation of FoxO by LRRK2 induces expression of proapoptotic proteins and alters survival of postmitotic dopaminergic neuron in drosophila. *Hum Mol Genet* **2010,** *19*, 3747-3758.

(11) Imai, Y.; Gehrke, S.; Wang, H. Q.; Takahashi, R.; Hasegawa, K.; Oota, E.; Lu, B. Phosphorylation of 4E-BP by LRRK2 affects the maintenance of dopaminergic neurons in drosophila. *EMBO J* **2008,** *27*, 2432-2443.

(12) Papkovskaia, T. D.; Chau, K. Y.; Inesta-Vaquera, F.; Papkovsky, D. B.; Healy, D. G.; Nishio, K.; Staddon, J.; Duchen, M. R.; Hardy, J.; Schapira, A. H.; Cooper, J. M. G2019S leucine-rich repeat kinase 2 causes uncoupling protein-mediated mitochondrial depolarization. *Hum Mol Genet* **2012,** *21*, 4201-4213.

(13) Heo, H. Y.; Kim, K. S.; Seol, W. Coordinate regulation of neurite outgrowth by LRRK2 and its interactor, rab5. *Exp Neurobiol* **2010,** *19*, 97-105.

(14) Gillardon, F. Leucine-rich repeat kinase 2 phosphorylates brain tubulin-beta isoforms and modulates microtubule stability: a point of convergence in parkinsonian neurodegeneration? *J Neurochem* **2009,** *110*, 1514-1522.

(15) Cirnaru, M. D.; Marte, A.; Belluzzi, E.; Russo, I.; Gabrielli, M.; Longo, F.; Arcuri, L.; Murru, L.; Bubacco, L.; Matteoli, M.; Fedele, E.; Sala, C.; Passafaro, M.; Morari, M.; Greggio, E.; Onofri, F.; Piccoli, G. LRRK2 kinase activity regulates synaptic vesicle trafficking and neurotransmitter release through modulation of LRRK2 macro-molecular complex. *Front Mol Neurosci* **2014,** *7*, 49.

(16) Schapansky, J.; Nardozzi, J. D.; Felizia, F.; LaVoie, M. J. Membrane recruitment of endogenous LRRK2 precedes its potent regulation of autophagy. *Hum Mol Genet* **2014,** *23*, 4201-4214.

(17) Lee, H.; James, W. S.; Cowley, S. A. LRRK2 in peripheral and central nervous system innate immunity: its link to Parkinson's disease. *Biochem Soc Trans* **2017,** *45*, 131-139.

(18) Le Grand, J. N.; Gonzalez-Cano, L.; Pavlou, M. A.; Schwamborn, J. C. Neural stem cells in Parkinson's disease: a role for neurogenesis defects in onset and progression. *Cell Mol Life Sci* **2015,** *72*, 773-797.

(19) Salado, I. G.; Zaldivar-Diez, J.; Sebastian-Perez, V.; Li, L.; Geiger, L.; Gonzalez, S.; Campillo, N. E.; Gil, C.; Morales, A. V.; Perez, D. I.; Martinez, A. Leucine rich repeat kinase 2 (LRRK2) inhibitors based on indolinone scaffold: Potential pro-neurogenic agents. *Eur J Med Chem* **2017,** *138*, 328-342.

(20) Noelanders, R.; Vleminckx, K. How Wnt signaling builds the brain: Bridging development and disease. *Neuroscientist* **2016**, 1-16.

(21) Lie, D. C.; Colamarino, S. A.; Song, H. J.; Desire, L.; Mira, H.; Consiglio, A.; Lein, E. S.; Jessberger, S.; Lansford, H.; Dearie, A. R.; Gage, F. H. Wnt signalling regulates adult hippocampal neurogenesis. *Nature* **2005,** *437*, 1370-1375.

(22) Ortega, F.; Gascon, S.; Masserdotti, G.; Deshpande, A.; Simon, C.; Fischer, J.; Dimou, L.; Chichung Lie, D.; Schroeder, T.; Berninger, B. Oligodendrogliogenic and neurogenic adult subependymal zone neural stem cells constitute distinct lineages and exhibit differential responsiveness to Wnt signalling. *Nat Cell Biol* **2013,** *15*, 602-613.

(23) Azim, K.; Fischer, B.; Hurtado-Chong, A.; Draganova, K.; Cantu, C.; Zemke, M.; Sommer, L.; Butt, A.; Raineteau, O. Persistent Wnt/beta-catenin signaling determines dorsalization of the postnatal subventricular zone and neural stem cell specification into oligodendrocytes and glutamatergic neurons. *Stem Cells* **2014,** *32*, 1301-1312.

(24) Piccin, D.; Morshead, C. M. Wnt signaling regulates symmetry of division of neural stem cells in the adult brain and in response to injury. *Stem Cells* **2011,** *29*, 528-538.

(25) Kurimoto, S.; Jung, J.; Tapadia, M.; Lengfeld, J.; Agalliu, D.; Waterman, M.; Mozaffar, T.; Gupta, R. Activation of the Wnt/beta-catenin signaling cascade after traumatic nerve injury. *Neuroscience* **2015,** *294*, 101-108.

(26) Libro, R.; Bramanti, P.; Mazzon, E. The role of the Wnt canonical signaling in neurodegenerative diseases. *Life Sci* **2016,** *158*, 78-88.

(27) L'Episcopo, F.; Tirolo, C.; Testa, N.; Caniglia, S.; Morale, M. C.; Serapide, M. F.; Pluchino, S.; Marchetti, B. Wnt/beta-catenin signaling is required to rescue midbrain dopaminergic progenitors and promote neurorepair in ageing mouse model of Parkinson's disease. *Stem Cells* **2014,** *32*, 2147-2163.

(28) Hussaini, S. M.; Choi, C. I.; Cho, C. H.; Kim, H. J.; Jun, H.; Jang, M. H. Wnt signaling in neuropsychiatric disorders: ties with adult hippocampal neurogenesis and behavior. *Neurosci Biobehav Rev* **2014,** *47*, 369-383.

(29) Berwick, D. C.; Harvey, K. LRRK2: an eminence grise of Wnt-mediated neurogenesis? *Front Cell Neurosci* **2013,** *7*, 82.

(30) Sancho, R. M.; Law, B. M.; Harvey, K. Mutations in the LRRK2 Roc-COR tandem domain link Parkinson's disease to Wnt signalling pathways. *Hum Mol Genet* **2009,** *18*, 3955-3968.

(31) Berwick, D. C.; Harvey, K. LRRK2 functions as a Wnt signaling scaffold, bridging cytosolic proteins and membrane-localized LRP6. *Hum Mol Genet* **2012,** *21*, 4966-4979.

(32) Berwick, D. C.; Javaheri, B.; Wetzel, A.; Hopkinson, M.; Nixon-Abell, J.; Granno, S.; Pitsillides, A. A.; Harvey, K. Pathogenic LRRK2 variants are gain-of-

function mutations that enhance LRRK2-mediated repression of beta-catenin signaling. *Mol Neurodegener* **2017,** *12*, 9.

(33) Harvey, K.; Outeiro, T. F. The role of LRRK2 in cell signalling. *Biochem Soc Trans* **2019,** *47*, 197-207.

(34) Chen, H.; Chan, B. K.; Drummond, J.; Estrada, A. A.; Gunzner-Toste, J.; Liu, X.; Liu, Y.; Moffat, J.; Shore, D.; Sweeney, Z. K.; Tran, T.; Wang, S.; Zhao, G.; Zhu, H.; Burdick, D. J. Discovery of selective LRRK2 inhibitors guided by computational analysis and molecular modeling. *J Med Chem* **2012,** *55*, 5536-5545.

(35) Lowery, R. G.; Majer, J. Assay Methods for Group Transfer Reactions. U. S. Patent 7,332,278, Nov 4, 2004.

(36) Correia Guedes, L.; Ferreira, J. J.; Rosa, M. M.; Coelho, M.; Bonifati, V.; Sampaio, C. Worldwide frequency of G2019S LRRK2 mutation in Parkinson's disease: a systematic review. *Parkinsonism Relat Disord* **2010,** *16*, 237-242.

(37) Deng, X.; Dzamko, N.; Prescott, A.; Davies, P.; Liu, Q.; Yang, Q.; Lee, J. D.; Patricelli, M. P.; Nomanbhoy, T. K.; Alessi, D. R.; Gray, N. S. Characterization of a selective inhibitor of the Parkinson's disease kinase LRRK2. *Nat Chem Biol* **2011,** *7*, 203-205.

(38) Di, L.; Kerns, E. H.; Fan, K.; McConnell, O. J.; Carter, G. T. High throughput artificial membrane permeability assay for blood-brain barrier. *Eur J Med Chem* **2003,** *38*, 223-232.

(39) Crivori, P.; Cruciani, G.; Carrupt, P. A.; Testa, B. Predicting blood-brain barrier permeation from three-dimensional molecular structure. *J Med Chem* **2000,** *43*, 2204-2216.

(40) Garcia-Velazquez, L.; Arias, C. The emerging role of Wnt signaling dysregulation in the understanding and modification of age-associated diseases. *Ageing Res Rev* **2017,** *37*, 135-145.

(41) Zhao, W.-N.; Cheng, C.; Theriault, K. M.; Sheridan, S. D.; Tsai, L.-H.; Haggarty, S. J. A high-throughput screen for wnt/β-catenin signaling pathway modulators in human iPSC-derived neural progenitors. *J Biomol Screening* **2012,** *17*, 1252-1263.

(42) Naujok, O.; Lentes, J.; Diekmann, U.; Davenport, C.; Lenzen, S. Cytotoxicity and activation of the Wnt/beta-catenin pathway in mouse embryonic stem cells treated with four GSK3 inhibitors. *BMC Res Notes* **2014,** *7*, 273.

(43) Fuentealba, L. C.; Obernier, K.; Alvarez-Buylla, A. Adult neural stem cells bridge their niche. *Cell Stem Cell* **2012,** *10*, 698-708.

(44) Ernst, A.; Alkass, K.; Bernard, S.; Salehpour, M.; Perl, S.; Tisdale, J.; Possnert, G.; Druid, H.; Frisen, J. Neurogenesis in the striatum of the adult human brain. *Cell* **2014,** *156*, 1072-1083.

(45) Biskup, S.; Moore, D. J.; Celsi, F.; Higashi, S.; West, A. B.; Andrabi, S. A.; Kurkinen, K.; Yu, S. W.; Savitt, J. M.; Waldvogel, H. J.; Faull, R. L.; Emson, P. C.; Torp, R.; Ottersen, O. P.; Dawson, T. M.; Dawson, V. L. Localization of LRRK2 to membranous and vesicular structures in mammalian brain. *Ann Neurol* **2006,** *60*, 557-569.

(46) Melrose, H. L.; Kent, C. B.; Taylor, J. P.; Dachsel, J. C.; Hinkle, K. M.; Lincoln, S. J.; Mok, S. S.; Culvenor, J. G.; Masters, C. L.; Tyndall, G. M.; Bass, D. I.; Ahmed, Z.; Andorfer, C. A.; Ross, O. A.; Wszolek, Z. K.; Delldonne, A.; Dickson, D. W.; Farrer, M. J. A comparative analysis of leucine-rich repeat kinase 2 (Lrrk2) expression in mouse brain and Lewy body disease. *Neuroscience* **2007,** *147*, 1047-1058.

(47) Gil-Perotin, S.; Duran-Moreno, M.; Cebrian-Silla, A.; Ramirez, M.; Garcia-Belda, P.; Garcia-Verdugo, J. M. Adult neural stem cells from the subventricular zone: a review of the neurosphere assay. *Anat Rec* **2013,** *296*, 1435-1452.

(48) Henderson, J. L.; Kormos, B. L.; Hayward, M. M.; Coffman, K. J.; Jasti, J.; Kurumbail, R. G.; Wager, T. T.; Verhoest, P. R.; Noell, G. S.; Chen, Y.; Needle, E.; Berger, Z.; Steyn, S. J.; Houle, C.; Hirst, W. D.; Galatsis, P. Discovery and preclinical profiling of 3-[4-(morpholin-4-yl)-7H-pyrrolo[2,3-d]pyrimidin-5-yl]benzonitrile (PF-06447475), a highly potent, selective, brain penetrant, and in vivo active LRRK2 kinase inhibitor. *J Med Chem* **2015,** *58*, 419-432.

(49) Sanchez-Mendoza, E. H.; Schlechter, J.; Hermann, D. M.; Doeppner, T. R. Characterization of seeding conditions for studies on differentiation patterns of subventricular zone derived neurospheres. *Front Cell Neurosci* **2016,** *10*, 55.

(50) West, A. B.; Moore, D. J.; Choi, C.; Andrabi, S. A.; Li, X.; Dikeman, D.; Biskup, S.; Zhang, Z.; Lim, K. L.; Dawson, V. L.; Dawson, T. M. Parkinson's disease-associated mutations in LRRK2 link enhanced GTP-binding and kinase activities to neuronal toxicity. *Hum Mol Genet* **2007,** *16*, 223-232.

(51) Ito, G.; Katsemonova, K.; Tonelli, F.; Lis, P.; Baptista, M. A.; Shpiro, N.; Duddy, G.; Wilson, S.; Ho, P. W.; Ho, S. L.; Reith, A. D.; Alessi, D. R. Phos-tag analysis of Rab10 phosphorylation by LRRK2: a powerful assay for assessing kinase function and inhibitors. *Biochem J* **2016,** *473*, 2671-2685.

(52) Eyers, P. A. 'Up with the LRRK': a phosphorylated Rab10 assay for evaluation of LRRK2 activity and inhibitor engagement. *Biochem J* **2016,** *473*, 2757-2762.

(53) Salado, I. G.; Redondo, M.; Bello, M. L.; Perez, C.; Liachko, N. F.; Kraemer, B. C.; Miguel, L.; Lecourtois, M.; Gil, C.; Martinez, A.; Perez, D. I. Protein kinase CK-1

inhibitors as new potential drugs for amyotrophic lateral sclerosis. *J Med Chem* **2014,** *57*, 2755-2772.

(54) Benek, O.; Hroch, L.; Aitken, L.; Gunn-Moore, F.; Vinklarova, L.; Kuca, K.; Perez, D. I.; Perez, C.; Martinez, A.; Fisar, Z.; Musilek, K. 1-(Benzo[d]thiazol-2-yl)-3-phenylureas as dual inhibitors of casein kinase 1 and ABAD enzymes for treatment of neurodegenerative disorders. *J Enzyme Inhib Med Chem* **2018,** *33*, 665-670.

(55) Karaman, M. W.; Herrgard, S.; Treiber, D. K.; Gallant, P.; Atteridge, C. E.; Campbell, B. T.; Chan, K. W.; Ciceri, P.; Davis, M. I.; Edeen, P. T.; Faraoni, R.; Floyd, M.; Hunt, J. P.; Lockhart, D. J.; Milanov, Z. V.; Morrison, M. J.; Pallares, G.; Patel, H. K.; Pritchard, S.; Wodicka, L. M.; Zarrinkar, P. P. A quantitative analysis of kinase inhibitor selectivity. *Nat Biotechnol* **2008,** *26*, 127-132.

(56) Schrödinger Release 2015-4 Protein Preparation Wizard; Epik version 3.4, S., LLC, New York, NY, 2015; Impact version 6.9, Schrödinger, LLC, New York, NY, 2015; Prime version 4.2, Schrödinger, LLC, New York, NY, 2015.

(57) Schrödinger Release 2015-4: Maestro, v., Schrödinger, LLC, New York, NY, 2015.

(58) Jorgensen, W. L.; Maxwell, D. S.; Tirado-Rives, J. Development and testing of the OPLS all-atom force field on conformational energetics and properties of organic liquids. *J Am Chem Soc* **1996,** *118*, 11225-11236.

(59) Schrödinger Release 2015-4: LigPrep, S., LLC, New York, NY, 2015.

(60) Schrödinger Release 2015-4: Glide, v., Schrödinger, LLC, New York, NY, 2015.

(61) https://www.discoverx.com/technologies-platforms/competitive-binding-technology/kinomescan-technology-platform (accessed Jul 8, 2019).

(62) Nieto-Estevez, V.; Oueslati-Morales, C. O.; Li, L.; Pickel, J.; Morales, A. V.; Vicario-Abejon, C. Brain insulin-like growth factor-I directs the transition from stem cells to mature neurons during postnatal/adult hippocampal neurogenesis. *Stem Cells* **2016,** *34*, 2194-2209.

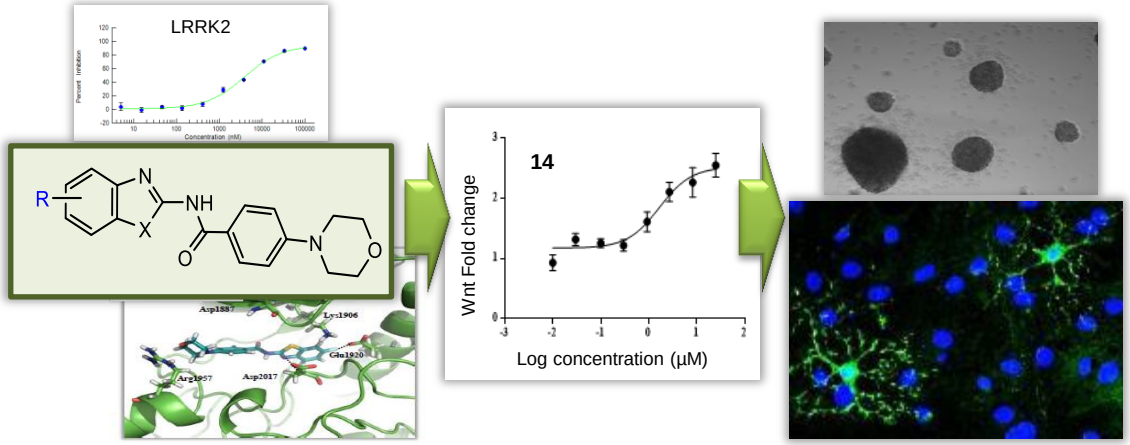
LRRK2
R
N
NH
X
O
N
O
Asp1887
Lys1906
Glu1920
Arg1957
Asp2017
14
Wnt Fold change
Log concentration (μM)